CIrrMap250: Annual maps of China's irrigated cropland from 2000 to 2020 developed through multisource data integration

Ling Zhang[1]*, Yanhua Xie[2], Xiufang Zhu[3], Qimin Ma[4], Luca Brocca[5]

[1]Key Laboratory of Remote Sensing of Gansu Province, Heihe Remote Sensing Experimental Research Station, Northwest Institute of Eco-Environment and Resources, Chinese Academy of Sciences, Lanzhou 730000, China

[2]Department of Geography & Environmental Sustainability, The University of Oklahoma, 100 East Boyd St, Norman, OK 73019, USA

[3]State Key Laboratory of Remote Sensing Science, Beijing Normal University, Beijing 100875, China

[4]College of Resources and Environment, Chengdu University of Information Technology, Chengdu 610225, China

[5]Research Institute for Geo-Hydrological Protection, National Research Council, Perugia 06128, Italy

Correspondence to: Ling Zhang (zhanglingky@lzb.ac.cn)

Abstract. Accurate maps of irrigation extent and dynamics are ~~important to study~~crucial for studying food security and its far-reaching impacts on Earth systems and the environment. While several efforts have been made to map irrigated ~~areas~~area in China, few ~~of them~~have provided ~~multi-year~~multiyear maps, incorporated national land surveys, addressed data discrepancies, and considered the ~~fraction~~fractional coverage of ~~irrigated~~cropland ~~(i.e., the mixed pixel issue). In this study~~within coarse-resolution pixels. Here, we addressed these important gaps and developed new annual maps of China's irrigated cropland from 2000 to 2020, named as CIrrMap250~~.~~ (China's irrigation map with a 250 m resolution). We harmonized ~~irrigated area~~irrigation statistics and ~~land~~surveys and reconciled them with remote sensing data. The refined estimates of irrigated area were then integrated with multiple remote sensing data (i.e., vegetation indices, hybrid cropland product, and paddy field maps) and an irrigation suitability map through a semi-automatic training approach. We ~~then~~evaluated our CIrrMap250 maps using ~~independently interpreted ~~~20,000 reference ~~locations~~samples, high-resolution irrigation water withdrawal data, and existing local to nationwide maps. ~~Our evaluation results showed that~~Our CIrrMap250 ~~agreed well with the reference points, with~~maps demonstrated an overall accuracy of 0.79-0.88 for ~~the ~~years 2000, 2010, and 2020, ~~respectively.~~and outperformed currently available maps. The CIrrMap250-estimated ~~irrigated~~irrigation area ~~can explain~~explained 50-60% of the variance in irrigation water ~~withdrawals~~withdrawal across China. ~~Our CIrrMap250 product showed superior performance than currently available ones (i.e., IrriMap_CN, IAAA, and GFSAD).~~CIrrMap250 revealed that China's ~~irrigated~~irrigation area has increased by about 180,000 km^2 (or 25%) from 2000 to 2020, with the majority (61%) ~~being~~occurring in the water-unsustainable ~~and occurring in~~regions facing ~~high to~~severe to extreme water stress. Moreover, our product unveiled a noticeable northward shift of China's ~~irrigated~~irrigation area, attributed to substantial ~~expansion~~expansions in irrigated cropland across Northeast and Northwest

China. The accurate representation ~~of~~ of irrigation ~~area~~extent in CIrrMap250 will greatly support hydrologic, agricultural, and climate studies in China ~~for~~, aiding in improved water and land resources management.

1 Introduction

Irrigation is increasingly important as an adaption strategy to climate change (Zaveri and B. Lobell, 2019; Bhattarai et al., 2023) and plays a vital role in ensuring food security by reducing both water and heat stresses of crops (Zhu and Burney, 2022; Zhu et al., 2022). ~~With~~Covering 20% of ~~spatial coverage in~~ global croplands ~~and providing~~, irrigated agriculture contributes to 40% of global food production (Unesco World Water Assessment Programme, 2019)~~, irrigated agriculture is a critical component of land and water resource management . Globally, agricultural irrigation accounts for~~. However, it uses 60-70% of total freshwater withdrawals and 80-90% of consumptive water uses (Qin et al., 2022; Wu et al., 2022). ~~Large volumes~~The extensive use of irrigation water use ~~intensify~~intensifies water management and ~~drive~~drives myriad Earth system and environmental impacts (Mcdermid et al., 2021; Mcdermid et al., 2023). These impacts include changes in hydroclimatic and biogeochemical cycling (Kang and Eltahir, 2018; Mishra et al., 2020; Thiery et al., 2020; Guo and Zhou, 2022; Yang et al., 2023), depletion of aquifers and surface water bodies (Cheng et al., 2014; Noori et al., 2021), freshwater salinization (Thorslund et al., 2021), and ~~landsides~~landslides (Lacroix et al., 2020). Given the vital importance of irrigation, ~~it is essential to know the exact~~knowing its precise location and ~~its'~~ dynamics~~, which, however, are~~ is essential. However, this proves challenging~~,~~ due to the hidden nature of irrigation signals and the frequent confusion between irrigated and rainfed fields (Ozdogan and Gutman, 2008; Zhang et al., 2022d; Chen et al., 2023).

Remote sensing provides significant opportunities for cost-effective and spatially explicit mapping of land surfaces (Potapov et al., 2021). ~~While numerous land use/cover and thematic cropland products have been made available to the public, they often lack information on irrigation status .~~ Over the past decade, there has been ~~a~~ growing interest in using ~~satellite~~ Earth observations to map irrigation ~~extents~~extent (Massari et al., 2021). ~~Currently,~~The existing remote sensing methods for irrigation mapping ~~irrigated areas~~are generally based on ~~satellite data can be broadly categorized into~~three indicators: vegetation~~-based~~ greenness, soil moisture~~-based~~, and integrated vegetation-soil moisture ~~integrated approaches. Various vegetation~~. Vegetation indices derived from optical sensors, such as the normalized difference vegetation index (NDVI) (Rouse et al., 1974), green index (GI) (Gitelson, 2005), and normalized difference water index (NDWI) (Gao, 1996; Mcfeeters, 1996), have been widely employed to detect irrigated areas ~~using~~based on the underlying fact that irrigated fields typically exhibit higher productivity and greenness compared to adjacent rainfed ones, especially under drought conditions. Techniques used include threshold splitting (Ozdogan et al., 2010; Zhu et al., 2014; Esmaeili et al., 2023; Wang et al., 2023)~~methods~~, spectral matching ~~techniques~~ (Ozdogan and Gutman, 2008; Lu et al., 2021), decision trees (Ozdogan and Gutman, 2008; Shahriar Pervez et al., 2014; Ambika et al., 2016; Xiong et al., 2017), and supervised classification (Deines et al., 2017; Deines et al., 2019; Xie et al., 2019)~~algorithms~~ . The ~~underlying principle of the vegetation~~soil moisture-based approach ~~is that irrigated fields typically exhibit higher productivity, greenness, and moisture content compared to adjacent rainfed areas, especially~~

under drought conditions. Moreover,~~under drought conditions. Moreover,~~utilizes remotely sensed soil moisture signals from microwave and optical sensors ~~has also been applied to detected irrigate~~ to detect irrigated areas by using similar techniques like threshold splitting ~~methods~~ (Yao et al., 2022)~~,~~ and supervised/unsupervised classification (Gao et al., 2018; Dari et al., 2021)~~algorithms , and remote sensing modeling comparison approaches .~~. The rationale behind ~~the soil moisture-based method~~this approach is that irrigation alters soil moisture ~~and leads~~, leading to distinct spatiotemporal dynamics compared to adjacent rainfed areas. ~~Additionally, the~~The vegetation-soil moisture ~~integrated~~integration approach~~, which~~ combines vegetation indices with soil moisture for ~~irrigated area~~irrigation detection~~,~~. This approach has ~~also~~ gained attention and achieved success in recent years (Pun et al., 2017; Elwan et al., 2022; Longo-Minnolo et al., 2022; Zuo et al., 2023)~~.~~, leveraging the strengths of both vegetation- and soil moisture-based methods for more accurate irrigation mapping.

Despite significant advancements ~~in remote sensing technique for irrigation~~, broad-scale mapping~~, identifying~~ of irrigated areas ~~at large spatial scales~~ (e.g., national and global levels) remains ~~a grand challenge~~challenging due to substantial variations in irrigation practices, ~~geographical~~landscapes, and climatic characteristics (Salmon et al., 2015; Zhang et al., 2022d). This challenge is further compounded by the lack of sufficient ground reference data (Xie et al., 2019; Xie and Lark, 2021). Consequently, high-~~precision irrigated area~~quality irrigation maps are still ~~lacking globally and~~missing in most countries (Chen et al., 2023; Mpakairi et al., 2023). In recent years, researchers have sought to address the challenges of large-scale irrigation mapping by integrating remote sensing data ~~with~~, agricultural statistics, existing irrigation maps, and other relevant datasets~~,~~ such as irrigation suitability (Meier et al., 2018; Xie et al., 2021; Zhang et al., 2022a; Zhang et al., 2022d)~~and existing irrigated area maps~~. They have successfully generated new irrigation maps at the global ~~or~~and national ~~scale~~scales, featuring higher ~~spatiotemporal~~spatial resolution and mapping accuracy compared to ~~previous~~existing products. These efforts underscore the great potential of multisource data~~-~~fusion techniques for large-scale irrigation mapping.

China is a big agricultural country with the largest irrigated area in the world (International Commission on Irrigation and Drainage, 2018)~~.~~. With only 8% of the world's ~~arable land~~cropland, China feeds 20% of the global population and has a tight connection with the food supply chain of other nations. Therefore, ~~the development of~~developing reliable maps of irrigated cropland is particularly important for sustainable food production in China. Despite this, less attention has been devoted to mapping ~~areas of~~ irrigated ~~cropland~~areas in China ~~than in~~compared to other countries with extensive irrigation, such as the United States and India (Zhu et al., 2014; Zhang et al., 2022d). It is only in recent years that ~~several~~ maps of irrigated cropland specifically tailored for China have emerged, facilitated by the integration of multisource data, including remote sensing, reported statistics, and existing ~~irrigation maps, and irrigation suitability~~land use/cover maps (~~Zhang et al., 2022c; Bai et al., 2022;~~Xiang et al., 2020; Bai et al., 2022; Zhang et al., 2022b; Zhang et al., 2022c; Zhang et al., 2022d).

While ~~these~~ previous studies have considerably improved our understanding of the spatial distribution of irrigated cropland in China, limitations remain. First, few studies ~~provide~~have provided annual irrigation maps ~~of irrigated cropland~~, hindering ~~a~~ spatiotemporal analysis of China's irrigated areas ~~in China~~. As a result, it remains unclear where the ~~expansion of irrigated~~changes in irrigation area ~~is~~are water-sustainable (~~i.e., irrigated area expanded~~e.g., irrigation expansion in ~~paces~~places without ~~experiencing~~ water stress) (Mehta et al., 2024). Second, ~~irrigated~~irrigation area data from official statistical bureaus,

~~which were~~ collected through field-sampling surveys ~~in conjunction with~~and bottom-up aggregation, have been extensively utilized to constrain the overall extent of irrigated cropland in previous studies. Besides statistical data, the National Land Surveys conducted by the State Council of China ~~actually~~ also ~~offer accurate and reliable information~~provide estimates on

100 irrigated cropland ~~areas~~acreage. The ~~National Land Surveys~~surveys involve ~~a great number of~~many investigators and ~~relies~~rely on ~~state of the art~~high-resolution satellite remote sensing imagery and advanced survey techniques (Chen et al., 2022). ~~The harmonization of irrigated area~~Harmonizing irrigation statistics with the National Land Surveys ~~might~~could potentially help to reduce biases and uncertainties ~~associated with irrigated area~~in each data source (Yu et al., 2021)~~,~~ but this has rarely been taken into account. Third, the majority of farms in China are small and fragmented, with the average farmland size being

105 ~~less~~smaller than a hectare (Teluguntla et al., 2018). This leads to the widespread presence of mixed pixels ~~in which both~~ where cropland and other land use/cover types ~~are present~~coexist. However, in most previous studies ~~described irrigated~~, binary cropland ~~in a Boolean fashion, where~~masks were used for irrigation mapping. These masks assign each pixel ~~is entirely occupied by~~as either ~~irrigated~~cropland or non-~~irrigated~~cropland~~.~~, neglecting the fractional coverage of cropland within coarse-resolution pixels. This may lead to overestimation or underestimation of ~~irrigated cropland, depending on the proportion of~~

110 ~~cropland within the grid cell.~~irrigation extent. Finally, it is worth noting that, apart from Zhang et al. (2022a)~~the study conducted by~~, many ~~other~~studies assessed their irrigation maps with a ~~relatively~~ limited number of reference samples, potentially compromising the reliability of their evaluation results (Zhu et al., 2014; Xiang et al., 2020; Bai et al., 2022; Zhang et al., 2022d)~~.~~. Obtaining ~~a~~sufficient ~~number of~~reference ~~points~~samples is crucial for ~~a~~robust ~~evaluation~~evaluations of national-scale irrigated cropland maps, a task that is, however, challenging due to the substantial cost and time involved.

115 Building on our previous work (Zhang et al., 2022d; Zhang et al., 2024), this study aims to bridge ~~the important~~these gaps ~~mentioned above~~and create new annual maps of irrigated cropland in China (2000-2020) by integrating ~~remotely sensed~~remote sensing data (i.e., vegetation indices, hybrid cropland ~~products~~maps, and paddy field maps), ~~irrigated area~~ reported statistics and surveys, and an irrigation suitability ~~to create new annual maps of irrigated cropland in China (2000-2020).~~map. The newly developed ~~irrigated cropland~~maps (~~named as~~CIrrMap250) ~~have~~feature a spatial resolution of 250

120 meters ~~and describe irrigated cropland distribution through fractional coverage. Our specific~~at an annual frequency from 2000 to 2020. Our maps show the percentage of each 250 m by 250 m pixel that is covered by irrigated cropland (i.e., pixel value = irrigated area / pixel area ×100). Other objectives of this study are: (i) ~~to assess~~assessing the accuracy of CIrrMap250 using ~~a sufficient number of referencing points~~~20,000 reference samples and high-resolution ~~data on~~irrigation water ~~withdrawals~~withdrawal data; (ii) ~~to compare~~comparing the performance of CIrrMap250 with ~~three~~four existing ~~large-

125 scale~~local to nationwide irrigation maps ~~that cover the entire China~~, including IrriMap_CN (Zhang et al., 2022a), IAAA (Siddiqui et al., 2016), ~~and~~ GFSAD (Thenkabail et al., 2016), ~~as well as a field scale map, i.e.,~~and OPTRAM30 (Yao et al., 2022); and (iii) ~~to investigate~~investigating the spatiotemporal dynamics of China's ~~irrigated cropland~~irrigation extent and ~~quantify~~quantifying the water sustainability of changes in irrigated area~~.~~.

2 Data acquisition and processing

2.1 Remote sensing data

We collected the Terra Moderate Resolution Imaging Spectroradiometer (MODIS) MOD13Q1 vegetation indices, i.e., NDVI and Enhanced Vegetation Index (EVI) (Huete et al., 1997), from the NASA's Earth Science Data Systems (https://www.earthdata.nasa.gov/). These indices are generated every 16 days with a 250 m spatial resolution. Meanwhile, the MODIS band 4 (545-565 nm) surface reflectance from the MOD09A1 product was used and resampled from the original 500 m to 250 m using the nearest neighbor interpolation method (Debeurs and Townsend, 2008). The resampled data were then used together with the 250-m and 8-day band 1 (620-670 nm) surface reflectance from MOD09Q1 to derive the Greenness Index (GI) (Supplementary Table S1). We extracted MODIS data for all cropland pixels in China, using only high-quality data on cloud- and snow/ice-free pixels (Hilker et al., 2012). Low-quality MODIS data were excluded based on the quality band and were interpolated using high-quality data from the neighboring cropland pixels.

We created a new 30 m resolution hybrid cropland product for China (CCropLand30) by fusing state-of-the-art remote sensing land use/cover products with the latest national land surveys (Zhang et al., 2024). CCropLand30 was generated at a 5-year interval from 2000 to 2020 and exhibited a higher accuracy compared to existing products (Zhang et al., 2024). Building upon CCropLand30, we developed 250-m resolution cropland layers for the years 2000, 2005, 2010, 2015, and 2020, which show the cropland proportion within each 250-m grid. Additionally, we extracted paddy fields from China's Land-use/cover dataset (CLUD) for the years 2000, 2005, 2010, 2015 and 2020 (Liu et al., 2014; Xu et al., 2018). Paddy fields, which include cultivated land where rice and lotus roots are grown and supported by water and irrigation facilities, were considered as part of irrigated cropland with high confidence (Zhang et al., 2022c).

2.2 Irrigation statistics and surveys

2.2.1 Harmonization of irrigation statistics and surveys

We collected annual irrigation area data (2000-2020) from various statistical yearbooks provided by the National Bureau of Statistics of China and local statistical bureaus. These yearbooks include the Provincial Statistical Yearbook, the Rural Statistical Yearbook, the China Statistical Yearbook for Regional Economy, and the China Water Statistical Yearbook. The data were sourced from the China Economic and Social Big Data Research Platform (https://data.cnki.net/). We compiled county-level irrigation

data for over 80% of provinces and prefecture-level data for the rest (Zhang et al., 2022d), which provide more detailed irrigation information for China than earlier studies (Zhu et al., 2014; Xiang et al., 2020; Zhang et al., 2022b).

In addition to statistical data, we utilized land survey data to obtain more detailed and reliable information on irrigated areas for select years. Currently, China has conducted three rounds of National Land Surveys in 1980s, 2010 and 2020, respectively. The surveys engaged a significant number of surveyors and utilized high-resolution satellite remote sensing imagery, along with advanced survey techniques like mobile internet, cloud computing, and drones (Chen et al., 2022). Due to national security concerns, the land survey maps were not publicly available. However, the Ministry of Natural Resource recently released county-level survey results of the second and third National Land Surveys, including data on cropland and its sub-categories (dryland, irrigated land, and paddy field) (https://www.mnr.gov.cn/). Within the dataset, the surveyed irrigated land and paddy field reflects the extent of irrigated cropland, covering the periods 2009-2016 and 2019-2022. For the years with survey data, irrigation statistics were harmonized with the survey data at the county scale using Eq. 1. The data harmonization was based on two assumptions: (1) the maximum value between statistical and surveyed irrigation area should be more reliable, and (2) irrigation area should be smaller than the total cropland area. The first assumption accounts for the underestimation tendency of both statistical and survey data due to possible insufficient and representative field sampling (Zhang et al., 2022a) and the prevalence of fragmented and small crop fields (Teluguntla et al., 2018). Alternative harmonization methods, such as mean and minimum values, were also tested but performed worse than the maximum harmonization approach. For years without survey data, the irrigation area was estimated by adjusting the harmonized data from adjacent survey years using relative change information derived from the irrigation statistics (Eq. 2). This method preserved the interannual changes observed in statistical irrigation area while enhancing data consistency across years.

$$A_{harm}^{ts} = min(max(A_{stat}^{ts}, A_{surv}^{ts}), CA_{surv}^{ts}) \tag{1}$$

$$A_{harm}^{t2} = min\left(A_{harm}^{ts} \times \left(1 + \frac{A_{stat}^{t2} - A_{stat}^{ts}}{A_{stat}^{ts}}\right), CA_{surv}^{ts}\right) \tag{2}$$

where A_{harm}, A_{stas} and A_{surv} represent the harmonized, statistical and surveyed irrigation area, respectively; CA is the surveyed area of cropland; and ts and $t2$ indicate the year with and without land surveys, respectively.

2.2.2 Reconciliation between statistical/~~surveyed~~survey data and remote sensing data

195 Cropland area statistics and survey data are inherently incompatible with remote sensing data due to ~~differences in~~different measurement techniques. ~~The former measures~~While statistical and survey data measure the net area of cropland, ~~while the latter~~remote sensing data represents the gross area of cropland ~~that includes~~, including subpixel, non-cropland features such as field ridges, linear elements, and scattered features ~~(e.g.,~~like roads, ponds, and rural houses~~)~~ (Zhang et al., 2024)~~. Consequently~~. As a result, statistical and surveyed cropland areas exhibit a negative and systematic bias compared to those derived from

200 remote sensing data (Zhang et al., 2021; Zhang et al., 2022d). ~~Irrigated cropland is~~Similarly, as a ~~part~~subset of cropland, ~~and its~~irrigated cropland is also reported as a net area in statistics and surveys ~~also indicate the net area of irrigated area. Consequently, a gap exists between the irrigated area from statistics/surveys and~~ that ~~derived~~is different from remote sensing data. ~~Direct use of~~Directly using the statistical~~/~~ or surveyed ~~irrigated~~irrigation acreage to constrain remote sensing-based irrigated cropland ~~extent~~would likely ~~leads to underestimation of irrigated croplands~~result in underestimating irrigation extent

205 (Schepaschenko et al., 2015). To ~~fill~~address this ~~gap~~discrepancy, we adjusted the harmonized ~~irrigated~~irrigation area ~~data~~ (Section 2.2.1) to reconcile the statistical~~/surveyed~~ and survey data with remote sensing data, as ~~seen~~shown in Eq. 3. This adjustment was ~~implemented under~~performed based on the assumption that the ~~irrigation~~ proportion of irrigated cropland remains consistent in ~~both~~the statistical/~~surveyed~~survey data and the remote sensing-derived maps. For ~~example~~instance, if ~~the~~statistical~~/~~ or survey data indicates a~~that~~ 99% ~~irrigation proportion~~of the cropland in ~~the croplands of~~ a given county is

210 irrigated, the remote sensing-derived irrigation proportion should also be ~~as high as~~approximately 99%.

$$A_{recon}^{t} = A_{harm}^{t} \times \frac{CA_{RS}^{t}}{CA_{surv}^{t}} \qquad (3)$$

-where A_{recon}^{t} and A_{harm}^{t} are the reconciled and harmonized ~~irrigated~~irrigation area, respectively, for the year t; CA_{RS}^{t} is the remote sensing-derived cropland area ~~that was~~ estimated from our hybrid cropland product (Zhang et al., 2024); CA_{surv}^{t} is the surveyed cropland area; $CA_{RS}^{t}/CA_{surv}^{t}$ ~~indicate~~denotes the bias ratio of remote sensing-derived cropland area relative to

215 surveys. This ratio was estimated for each county and constrained to the median value of all counties in its agricultural zones (Zhang et al., 2022c) to exclude extreme bias ratios and to ensure a conservative adjustment. In years lacking survey data, the bias ratio was estimated using a straightforward nearest-neighbor interpolation method.

2.3 Auxiliary data

220 This study utilized various auxiliary datasets~~,~~ (Supplementary Table S2), including meteorological and environmental variables, irrigation water withdrawal, water scarcity index, and administrative boundaries. Daily meteorological observations~~, including~~ such as precipitation, relative ~~humility~~humidity, air temperature and pressure~~, at~~ were collected from approximately 2400 meteorological stations ~~were collected from~~across China, provided by the National Meteorological Information Center (NMIC, http://data.cma.cn/). These datasets were ~~used in combination~~combined with the MCD43A3 albedo product ~~for the~~

225 to compute daily potential evapotranspiration (PET) using the Priestley-Taylor method (Priestley and Taylor, 1972). The daily PET values were aggregated to annual values for the period from 2000 to 2020, which were then used to derive the aridity index (defined as the ratio of precipitation to PET). The environmental variables included elevation, slope, cropping intensity, soil type, and distance to water bodies. Elevation data was sourced from the Shuttle Radar Topography Mission digital elevation model (SRTM DEM), and the slope

230 map was generated from the SRTM DEM data using the slope function in ArcGIS. The distance to water bodies was calculated based on the spatial distribution of water bodies (rivers, lakes, reservoirs, canals, and ponds) using the Euclidean distance tool in ArcGIS. The above auxiliary data were partly obtained from the National Tibetan Plateau (https://data.tpdc.ac.cn/) and the remaining from the Resource and Environment Science and Data Center

235 (https://www.resdc.cn/Default.aspx).

Additionally, the prefecture-level irrigation water withdrawal data for 2009-2011 and 2018-2020 were compiled from provincial water resources departments and local statistical bureaus. The prefecture-level data on water scarcity index (WSI) for 2010-

240 2020 were extracted from our previous study (Zhang et al., 2023b). WSI is defined as the ratio of total water use to water availability, as shown in Supplementary Table S2. Total water use encompasses both groundwater and surface water withdrawals for irrigation, industry, domestic purposes, forestry, livestock, and fishery. Water availability refers to the total surface water and groundwater generated by precipitation.

245 **3 Methodology**

In this study, we created annual maps of irrigated cropland in China by integrating multisource data through a semi-automatic training approach (Xie et al., 2019; Zhang et al., 2022d). After acquiring and processing the data, our methodology started with the creation of training samples, as depicted in Figure 1. This step involves three major processes: (i) generating intermediate irrigation maps through a threshold-calibration

250 method; (ii) establishing a training pool (i.e., potential training data) via overlay analysis of the intermediate maps; and (iii) generating training samples through random sampling from the training pool. Using these training samples, we classified irrigated and rainfed cropland in each county annually using the random forest algorithm (Breiman, 2001). The resulting county-level maps were then mosaicked and post-processed to produce the annual maps of irrigated cropland in China, referred to as CIrrMap250. Subsequently,

255 we evaluated the accuracy of CIrrMap250, and compared it with existing

products. ~~Lastly~~Finally, we examined the spatiotemporal changes in irrigated croplands and quantified the water sustainability of irrigation ~~area~~ expansion by ~~comparing it~~relating them with water stress areas.
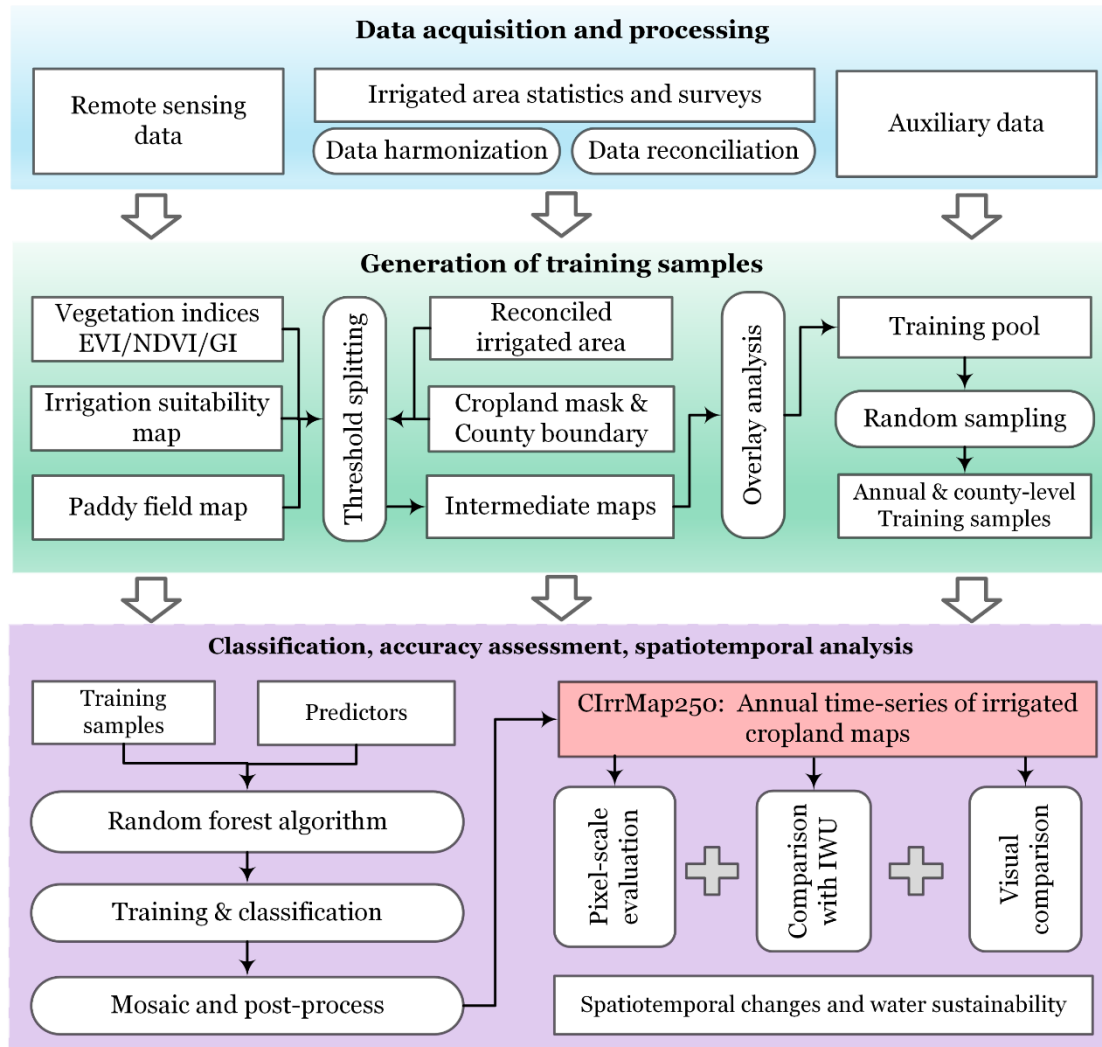
Figure 1. Workflow of this study

260

3.1 Generation of training samples

~~A~~We applied a threshold-calibration method ~~was applied~~ to automatically generate the training pool ~~for irrigated and rainfed cropland~~, following ~~the~~ previous studies by Xie et al. (2019; 2021) and Zhang et al. (2022d)~~. We~~. With this method, cropland pixels with annual peak vegetation greenness exceeding an optimized threshold were classified as "irrigated". The threshold

265   was individually calibrated for each county and year using available irrigation statistics and surveys. Based on the calculated optimized thresholds, intermediate irrigation maps were generated at the county level. Pixels consistently classified as

"irrigated" in all intermediate maps were identified as irrigation candidates, while those classified as "non-irrigated" were considered potential non-irrigated samples.

270   In this study, we first calculated the peak ~~vegetation index~~values of vegetation indices (NDVI, EVI, and GI) for cropland grids in each year and adjusted ~~it~~them by irrigation suitability. ~~The growth-period peak values of NDVI, EVI, and GI were determined for cropland grids in each year.~~ A static irrigation suitability map ~~were constructed~~was created based on ~~the~~ elevation, slope, and aridity index of cropland~~. As demonstrated by , these~~. These factors ~~are pivotal~~play a crucial role in ~~influencing~~shaping the spatial distribution of irrigated cropland in China, as demonstrated by Liu et al. (2022)~~.~~. Cropland ~~with~~ areas characterized by lower elevation, gentler ~~slope~~slopes, and higher aridity ~~index was~~indices were hypothesized to ~~have~~

275 ~~higher~~exhibit greater irrigation suitability and potential, in line with previous studies (Worqlul et al., 2015; Worqlul et al., 2017; Li and Chen, 2020; Zhang et al., 2022d)~~.~~. Specifically, the ~~cropland~~ irrigation suitability map was derived by combining ~~the~~ irrigation suitability values of elevation, slope, and aridity index, as in Eq. ~~3~~4.

$$S_{i,j,k} = \frac{1}{4}w_{1,k}SElev_{i,j} + \frac{1}{4}w_{2,k}SSlope_{i,j} + \frac{1}{10}w_{3,k}SArid_{i,j} \qquad (\text{\sout{3}}4)$$

where $S_{i,j,k}$ is the irrigation suitability for cropland cell i in county j of province k; w is the weight of the influencing factors,

280 which was determined ~~by~~through a trial-and-error procedure; $SElev$, $SSlope$, and $SArid$ are the irrigation suitability values of elevation, slope, and aridity index, respectively (Supplementary Table ~~S2~~S3). The peak vegetation index was subsequently adjusted by irrigation suitability (Eq. ~~4), which~~5), with the assumption that irrigated cropland ~~is not only~~, being greener and more productive ~~but~~, is also more suitable for irrigation ~~than~~compared to rainfed cropland.

$$SVI_{i,j,k}^{t} = S_{i,j,k} \times Peak\,(VI_{i,j,k}^{g,t}) \qquad (\text{\sout{4}}5)$$

285 where SVI denotes the irrigation suitability-adjusted peak vegetation index; VI denotes the ~~value of~~ vegetation index~~,~~ value; g and t represent the growth period and year, respectively.

       We then generated three intermediate irrigation maps ~~for each year~~annually from 2000 to 2020 utilizing the SVI (i.e., irrigation suitability-adjusted peak NDVI, EVI, and GI) and the paddy field maps. This was ~~accomplished~~achieved through a threshold splitting method (Pervez and Brown, 2010; Zhu et al., 2014; Meier et al., 2018). Specifically, the SVI values for all

290 ~~croplands~~cropland pixels within each county were ranked in a descending order~~ within each county~~, and the cumulative irrigated area was sequentially ~~estimated. Subsequently, the~~calculated. The accumulated area was then compared with the reconciled ~~irrigated~~irrigation area. The SVI value ~~corresponding to the grid where~~at which the cumulative irrigated area closely matched the reconciled irrigated area was ~~determined~~identified as the optimal threshold~~ value~~. Notably, for paddy fields, the SVI value was set to the maximum SVI ~~of the~~among croplands ~~in~~within a ~~given~~ county, prioritizing ~~it as irrigated~~these areas

295 as "irrigated". The ~~croplands~~cropland grids were finally classified into "irrigated" and "rainfed" categories using Eq. ~~5~~6.

$$cropland_{i,j,k} = \begin{cases} irrigated_{i,j,k}^{t} & SVI_{i,j,k}^{t} \geq threshold_{j,k}^{t} \\ rainfed_{i,j,k}^{t} & SVI_{i,j,k}^{t} < threshold_{j,k}^{t} \end{cases} \qquad (\text{\sout{5}}6)$$

The intermediate irrigation maps were finally overlaid to identify pixels consistently classified as irrigated or rainfed cropland across these maps. These pixels were designated as potential training samples, forming the training pool for each county and year. From the training pool, we randomly selected 200 rainfed pixels and 200 irrigated pixels to train the random forest model. This selection ensures a balance between the need for an adequate number of samples and the computational efficiency of the classification algorithm (Xie et al., 2019; Zhang et al., 2022d).

3.2 Classification of irrigated cropland using random forest

We employed the random forest algorithm (Breiman, 2001) to classify irrigated and rainfed cropland using the random samples extracted from the training pool. The hyperparameters of our model were optimized through a trial-and-error process, including the number of trees, the minimum number of observations per node, and the number of variables randomly sampled at each decision split (Supplementary Table S4). The input features of our model encompassed both time-varying variables (i.e., vegetation indices, precipitation, temperature, PET, and aridity index) and stable environmental variables (i.e., latitude, longitude, cropping intensity, elevation, distance to water bodies, slope, and soil type). The classification was conducted independently for each county per year from 2000 to 2020. After that, we merged the annual, county-level mapping results to generate preliminary binary irrigation maps in China (i.e., 1 for "irrigated" and 0 for "non-irrigated").

We then employed a spatial filtering to remove isolated irrigation pixels and identify potentially omitted irrigated croplands. Specifically, we first calculated the irrigation proportion within a 7×7-pixel window for each preliminary irrigation pixel. Then, all cropland pixels within the moving window were assigned as "non-irrigated" if the calculated ratio fell below 5%. Conversely, if the ratio exceeded 95%, we assumed all cropland pixels within the moving window to be irrigated. The spatial filtering operation preserved the original spatial resolution of the maps (250 m).

Finally, we multiplied the binary, spatially filtered irrigation maps by each corresponding cropland mask layers to generate annual irrigation maps for China. The final product, CIrrMap250, represents the percentage of a 250 m pixel covered by irrigated croplands (i.e., pixel value = irrigated area / pixel area ×100). Unlike simple binary maps, our product considers the fractional coverage of croplands within coarse-resolution MODIS pixels, thereby enhancing the accuracy of irrigation area estimates in China, where farms are typically small and fragmented.

3.3 Accuracy assessment and inter-comparison

~~The accuracy of CIrrMap250 was assessed from three distinct perspectives. First, pixel scale accuracy was evaluated using over 20,000 reference points collected from existing literatures and land use maps of the National Land Survey in China. Furthermore, the performance of CIrrMap250 was indirectly assessed by comparing its irrigated area estimates with high-resolution data on irrigation water withdrawal. In addition, we compared CIrrMap250 with three currently available large-scale irrigation maps, i.e., IrriMap_CN , IAAA , and GFSAD , as well as a field scale (30 m resolution) map in the Hexi Corridor of Northwest China (Yao et al., 2022).~~

3.3.1 Assessment with reference points

We assessed the accuracy of CIrrMap250 using three independent ~~datasets~~sets of validation samples ~~(Figure 2)~~. The first validation ~~samples~~dataset was for the year 2000 ~~were~~(Figure 2a), obtained from Zhu et al. (2014), ~~which were~~ primarily derived from the crop growth and soil moisture dataset provided by the China Meteorological Data Sharing Service System (https://data.cma.cn/). The second validation ~~samples~~dataset, for the year 2020 ~~were acquire~~(Figure 2c), was acquired from Chen et al. (2023), ~~who mapped~~ that showed the global location of center pivot irrigation systems (CPIS~~) in global arid regions. The CPIS are characterized by a circular irrigation pattern centered on pivots, which creates a distinct circular pattern on the crop (Figure 2c). This characteristic enables a reliable identification of the CPIS from remote sensing images.~~). We extracted the CPIS polygons across China (mainly distributed ~~throughout China and converted them into validation points (i.e., the center of each CPIS polygon), which are mainly located in~~ in the Northern China~~.~~) and compared with our product. In addition, we retrieved the validation samples for the year circa 2010 (Figure 2b) from the provincial land-use maps of ~~the~~China's second National Land Survey ~~in China~~ (https://www.mnr.gov.cn/). ~~Due to the lack of georeferencing information, we~~We georeferenced these land use maps using the georeferencing tool in ArcGIS ~~in conjunction with~~. A total of 234 control points were selected from high-resolution images~~. The irrigated~~ and provincial administrative boundaries for the georeferencing process (Supplementary Figure S1). The irrigation samples were ~~taken~~randomly extracted from ~~the patches of~~ irrigated lands and paddy fields ~~in the georeferenced land use maps~~, while non-irrigated samples were taken from dryland patches. ~~Note that the surveyed land use maps of the third National Land Survey are not available currently. In total, we~~As shown in Figure 2d, we totally obtained ~~a more than~~ 20,~~000~~720 reference samples~~, enabling a robust assessment of the irrigation maps.~~

The performance of CIrrMap250 was evaluated quantitively using the overall accuracy (OA), F1-score, producer's accuracy (PA), and user's accuracy (UA) (Supplementary Table ~~S4). CIrrMap250 describes irrigated cropland distribution through fractional coverage rather than in a binary manner. The pixel values in CIrrMap250 indicate the percentage of irrigated cropland within each grid cell. It's noteworthy that this percentage represents the proportion of cropland within the 250-meter grid cell (estimated from the 30-meter hybrid cropland product), not the proportion of irrigated cropland to total cropland. Essentially, the cropland area within each 250-meter grid cell is categorized as either "irrigated" or "non-irrigated". Hence, for pixel-scale accuracy evaluation, CIrrMap250 was converted into binary maps, whereby pixels with values greater than 0 were coded as 1, representing irrigated cropland, while other pixels were coded as 0, representing non-irrigated area.~~ S5).
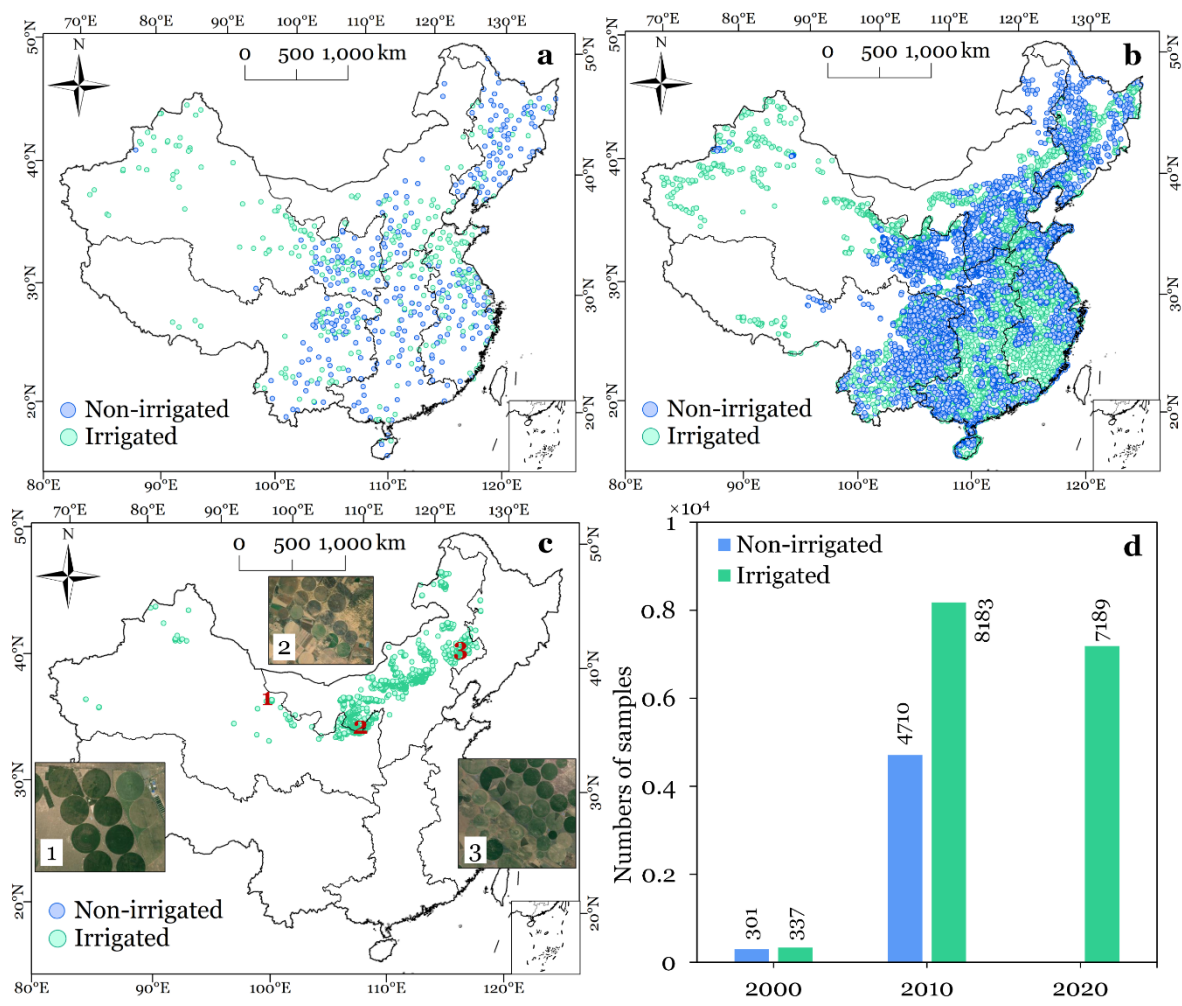
Figure 2. Spatial distribution of validation samples. a, Spatial distribution of the third-party samples in 2000. **b**, Spatial distribution of the samples in 2010 retrieved from provincial land-use maps of China's second National Land Survey. **c**, Spatial distribution of the third-party samples in 2020. **d**, Numbers of irrigated and non-irrigated samples for different years.

3.3.2 Assessment with irrigation water withdrawal data

We further assessed the performance of CIrrMap250 by comparing its ~~irrigated~~irrigation area ~~estimates~~ with ~~high resolution~~ (prefecture-level~~)~~ ~~data on~~ irrigation water ~~withdrawals~~withdrawal for the years circa 2010 and 2020. ~~Irrigated~~Since irrigated area is a ~~major~~dominate driver ~~to~~of irrigation water withdrawal (Lamb et al., 2021; Puy et al., 2021)~~. Therefore,~~, irrigation water withdrawal can indirectly ~~validate~~evaluate the accuracy of irrigation maps (Zhang et al., 2022a). ~~A more accurate irrigated cropland map is~~High-accuracy irrigation maps are expected to ~~exhibit a more robust correlation between its irrigated~~better explain the variations in irrigation water withdrawal compared to low-accuracy maps. The explanatory power

380 of the irrigation area estimates. The strength of this correlation was assessed by the coefficient of determination (R^2) from a linear regression model fitted to the irrigation water withdrawal data using the least squares method.

3.3.3 Comparison with existing products

385 We evaluated CIrrMap250 using three existing irrigation maps covering the entire China, including IrriMap_CN (Zhang et al., 2022a), IAAA (Siddiqui et al., 2016), and GFSAD (Thenkabail et al., 2016). IrriMap_CN provides annual irrigation maps across China for the years from 2000 to 2019 at a 500 m resolution, which was developed using MODIS data and machine learning (Zhang et al., 2022a). The 390 IAAA irrigation maps cover Asia and Africa for the years 2000 and 2010 at a 500 m resolution. These maps were created based on seasonal vegetation variations captured in MODIS data (Siddiqui et al., 2016). The 2010 global irrigation map, GFSAD, has the spatial resolution of 1000 m and was generated by overlaying remote sensing-derived irrigated and rainfed cropland map (Thenkabail et al., 2016).

395   Additionally, we evaluated our maps for the Hexi Corridor using a field-scale irrigation map. OPTRAM30 was specifically created for the region (Yao et al., 2022). The map, OPTRAM30, has a 30 m resolution and demonstrates an accuracy close to 100% when validated against in situ datasets. In addition 400 to assessing CIrrMap250, we also evaluated IrriMap_CN, IAAA, and GFSAD using OPTRAM30.

3.4 Irrigation area change and its correlation with water stress areas

405 We examined the irrigation trends in a spatially explicit manner using our new irrigation maps from 2000 to 2020. The trends were quantified as the slope of the regression line fitted to the time-series irrigation data at the pixel scale using the least squares method. Furthermore, we adopted the concept of "center of gravity" to track the spatial dynamics of irrigated areas (Zeng and Ren, 2022). The gravity center of irrigated area (X, Y) is represented as:

$$X^t = \frac{\sum_{i=1}^{n} IrrArea_i^t \times x_i}{IrrArea_i^t} \tag{7}$$

$$Y^t = \frac{\sum_{i=1}^{n} IrrArea_i^t \times y_i}{rrArea_i^t} \qquad (~~7~~8)$$

where $IrrArea_i^t$ denotes the irrigated area in grid i; x_i and y_i are the longitude and latitude of grid i, respectively; n is the number of irrigated cropland grids; and t is year.

In addition, we quantified ~~the~~ water sustainability of ~~changes in~~ irrigation ~~areas. The~~changes across China. To do so, we first identified the expansion and decline in irrigated areas between 2000 and 2020 ~~were first identified at the pixel scale. To better visualize the results, we aggregated changes in irrigated area to~~at a 5- km resolution, following previous studies (Deines et al., 2019; Xie and Lark, 2021). ~~~~Subsequently, we compared ~~these~~the changes with a prefecture-level water stress map derived from the mean values of WSI over the period 2010-2020. ~~The~~WSI denotes the fraction of available water resources appropriated by humans and is employed to categorize water stress ~~across different prefectures~~into four levels: low (WSI~~≤~~ ≤ 0.2), moderate (0.2~~<~~ < WSI ≤0.4), ~~high~~severe (0.4 < WSI~~≤~~ ≤ 1.0), and ~~severe~~extreme (WSI~~>~~ > 1) (Zhang et al., 2023b)~~. Expansions of irrigated areas~~. Irrigation expansion under severe to extreme water stress ~~were~~was designated as "unsustainable" due to ~~their~~the potential ~~to exacerbate the~~of exacerbating depletion of surface water and groundwater (Mehta et al., 2024)~~resources~~. Conversely, the expansion of ~~irrigated aeras~~irrigation under low to moderate water stress, or ~~reductions in irrigated areas~~the shrinkage of irrigation under severe to extreme stress ~~were~~was deemed "sustainable".

4 Results

4.1 Accuracy assessment ~~of irrigated cropland maps~~

4.1.1 Pixel-scale assessment

As ~~depicted~~shown in Figure 3 and Supplementary Table ~~S5~~S6, CIrrMap250 attains an OA and F1-score of 0.79 and 0.78, respectively, for the year 2000, surpassing the performance of IrriMap_CN and IAAA. In the year 2010, CIrrMap250 achieves a high OA of 0.79 and a F1-score of 0.71, whereas the existing maps attain OA values below 0.66 and F1 scores under 0.63. For the year 2020, CIrrMap250 detects 88% of ~~the fields with~~ center pivot ~~irrigation systems~~irrigated fields, while IrriMap_CN identifies only 20% (Figure 3c and Supplementary Figure ~~S1).~~S2). Note that both CIrrMap250 and IrriMap_CN achieves a perfect user's accuracy in 2020 mainly because all the reference points are irrigated samples (Section 3.31 and Supplementary Table S7). For irrigated samples, CIrrMap250 has significantly higher producer's accuracy in 2000, 2010, and 2020, compared to the existing products. CIrrMap250 and IrriMap_CN performs similarly in user's accuracy. For non-irrigated samples, the producer's accuracy of CIrrMap250 is ~~relatively~~slightly lower than that of IrriMap_CN, but the user's accuracy is significantly higher than that of IrriMap_CN. In terms of producer's accuracy and user's accuracy, both CIrrMap250 and IrriMap_CN ~~obviously~~ outperform IAAA and GFSAD.

440
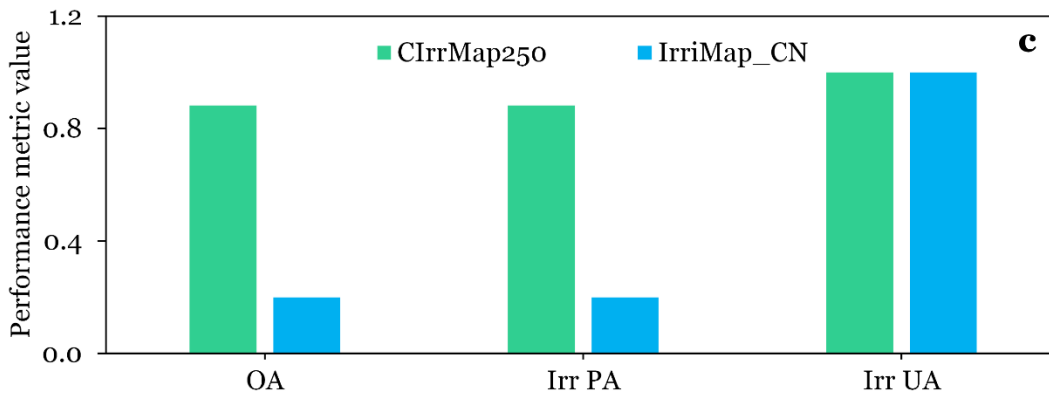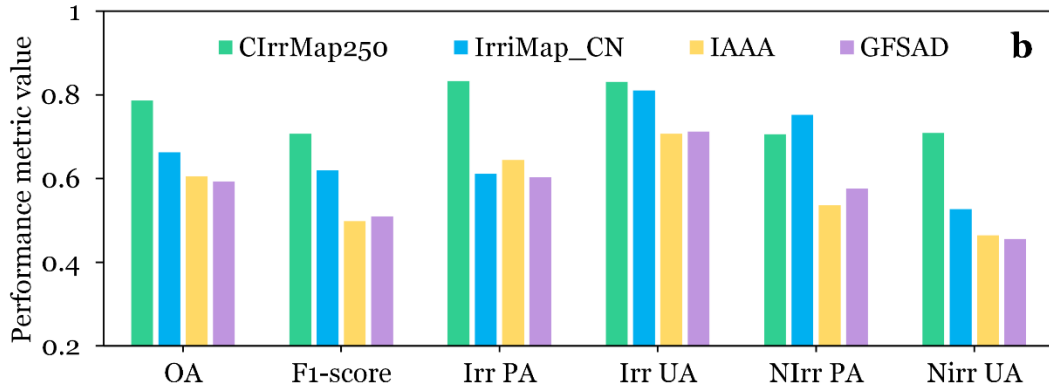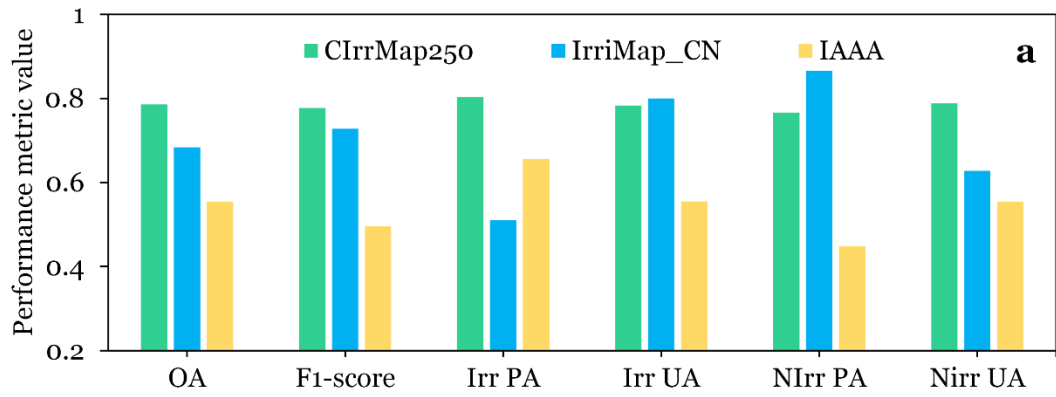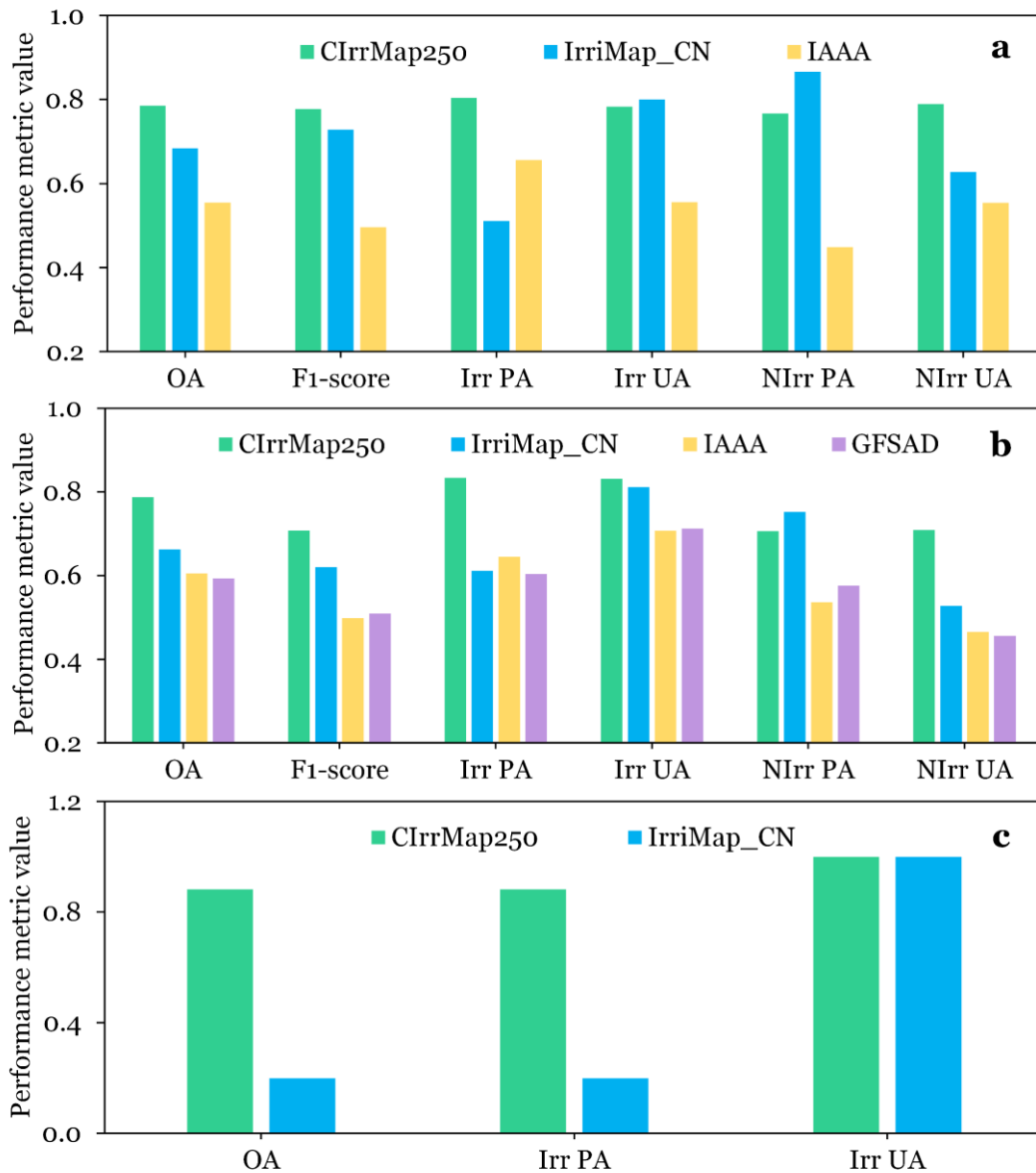
Figure 3. Performance of CIrrMap250 and ~~the~~ existing irrigation maps (IrriMap_CN, IAAA, GFSAD). Panels **a**, **b** and **c** show the results for 2000, 2010, and 2020, respectively. OA, PU, and UA ~~are~~represent overall accuracy, producer's accuracy, and user's accuracy, respectively. Irr and NIrr indicate irrigated and non-irrigated samples, respectively.

4.1.2 Nationwide and regional comparison with existing products

Figure 4 ~~compares~~shows the spatial distribution of irrigated cropland ~~in CIrrMap250 with the existing~~from different maps. At the national scale, CIrrMap250 and IrriMap_CN, specifically developed for China, ~~can~~ capture similar irrigation patterns. ~~Irrigation~~They both show some irrigation hotspots (e.g~~.,~~, North China Plain and Northwest China) and well-known irrigation districts like Hetao, Baojixia, Dujiangyan, Qingtongxia, and Fenhe ~~are consistently identified by these maps. The irrigated croplands depicted by~~. However, CIrrMap250 ~~are~~shows more ~~widely distributed~~widespread irrigation than ~~those portrayed by~~IrriMap_CN ~~across the majority~~in most areas of China (Supplementary Figure ~~S2). CIrrMap250 yields~~S3). IrriMap_CN estimates irrigation ~~ratios~~proportion (i.e., the ratio of irrigated cropland area to ~~the~~total cropland area) ~~of~~to be 0.~~58~~47, 0.~~70~~37, and 0.~~96, respectively,~~61 for China, Northern China, and Xinjiang Uygur Autonomous Region~~. These values~~, respectively (Supplementary Figure S4). In comparison, the values derived from CIrrMap250 are 0.58, 0.70, and 0.96, respectively, which align more closely with the ~~reality and the~~official ~~report~~reports (https://gtdc.mnr.gov.cn/~~), in comparison to those derived from IrriMap_CN, which are only 0.47, 0.37, 0.61, respectively (Supplementary Figure S2). However~~). Nevertheless, CIrrMap250 tends to yield lower estimates of irrigation area in Northeast China (NEC) when compared to IrriMap_CN~~.~~, possibly due to inaccurate statistical and survey data in this region. In contrast to CIrrMap250 and IrriMap_CN, IAAA notably underestimates irrigated croplands in Northwest China (NWC) and North China (NC), but overestimates ~~them~~in NEC and Southwest China (SWC). This could be explained by the fact that IAAA was developed using unsupervised classification (Siddiqui et al., 2016), limiting its ability to characterize the spatial heterogeneity of irrigation in China (Tian et al., 2024). GFSAD shows overestimations of irrigated area in the Dujiangyan district and the North China Plain~~,~~ but exhibits evident omission errors in sparsely distributed irrigation regions like NWC and ~~the southern part of~~South China (SC). The large bias of GFSAD is understandable, as it is not an irrigation-specific product and only covers five irrigated crops(Thenkabail et al., 2016; Xie et al., 2021).
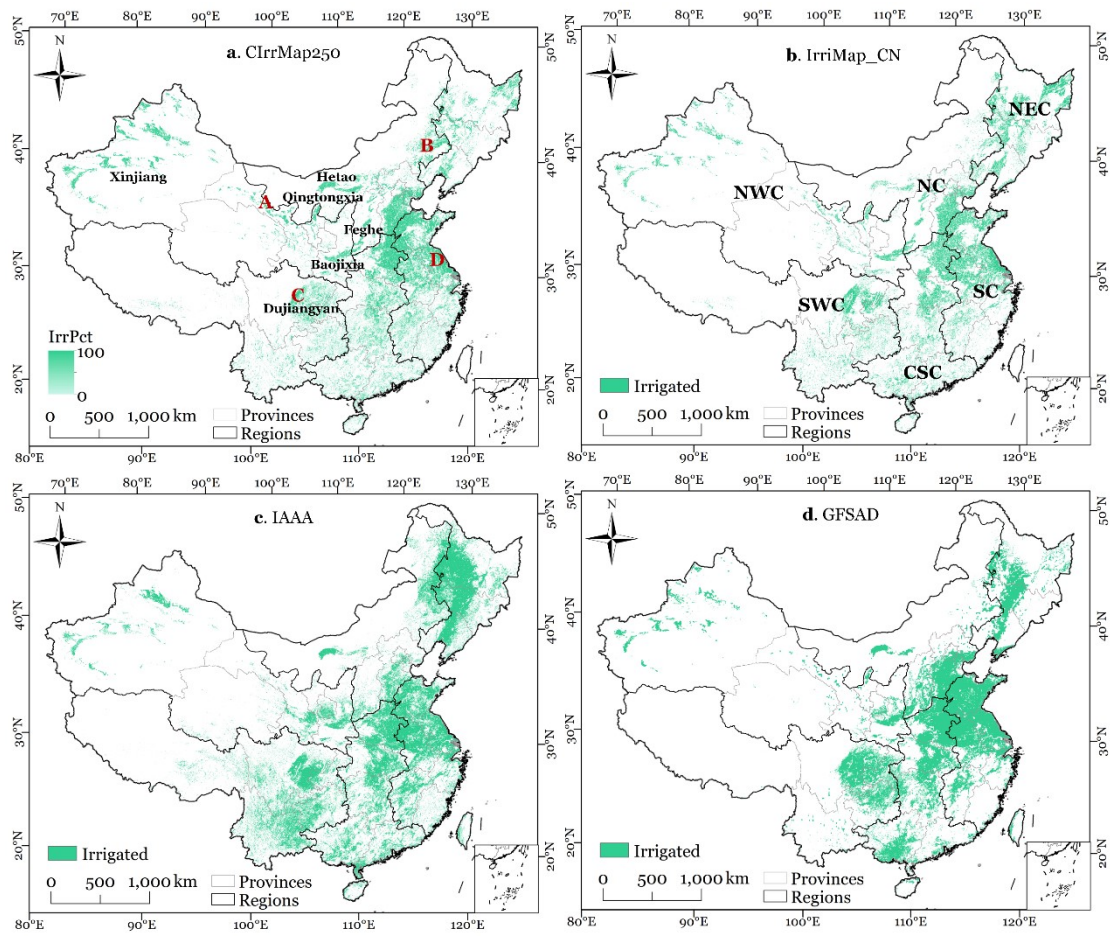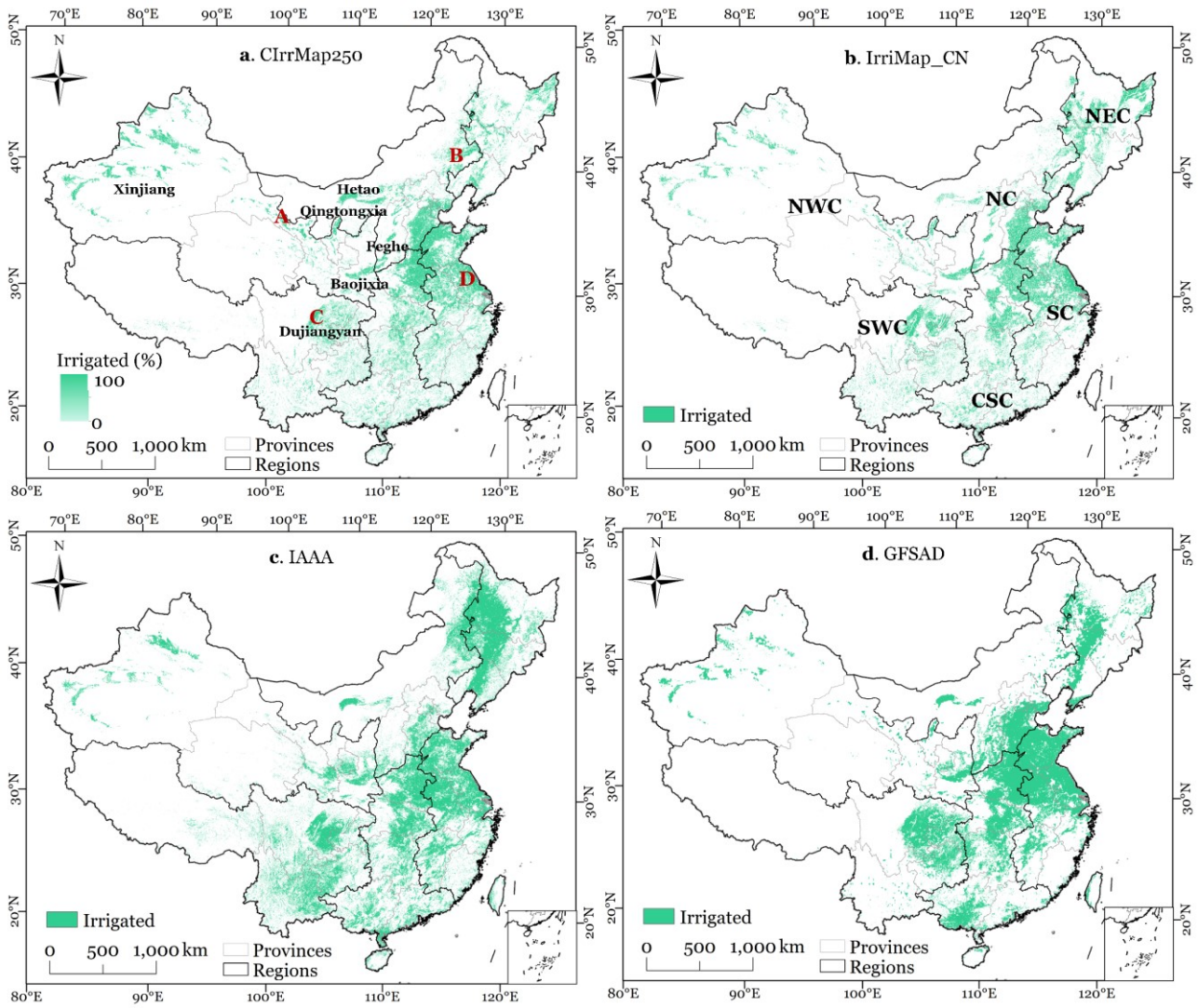
Figure 4. Spatial distribution of irrigated cropland ~~in~~from different ~~irrigation~~ maps for the year 2010. NEC, NC, NWC, SWC, SC and CSC ~~are the abbreviations of~~represent Northeast China, North China, Northwest China, Southwest China, South China, and Central South China. ~~IrrPct represents the proportion of irrigated cropland relative to the total area of a grid cell.~~, respectively.

We further compared CIrrMap250 with ~~the~~ existing maps in four heavily irrigated zones (A-D locations are shown in Figure 4a). Zones A and B are situated in arid regions where crop growth ~~depends greatly on~~is not possible without irrigation, while ~~Zones~~zones C and D are ~~located~~ in humid regions where paddy rice is ~~extensively cultivated~~widespread and relies heavily on supplemental irrigation. As ~~depicted~~shown in Figure 5, CIrrMap250 accurately portrays the actual distribution of irrigated cropland in these zones. In contrast, IrriMap_CN underestimates irrigation extent in zones A and B and lacks detailed information ~~on irrigated cropland~~ in zones C and D. IAAA significantly underestimates ~~the irrigated~~irrigation area in zone A,

incorrectly identifies ~~irrigated cropland~~ in zone B, and overestimates irrigated cropland in region C. The GFSAD product, with a relatively coarse resolution of 1 ~~kilometer, has~~km, shows the lowest agreement with ~~the distribution of actual irrigated cropland among the four~~other maps.
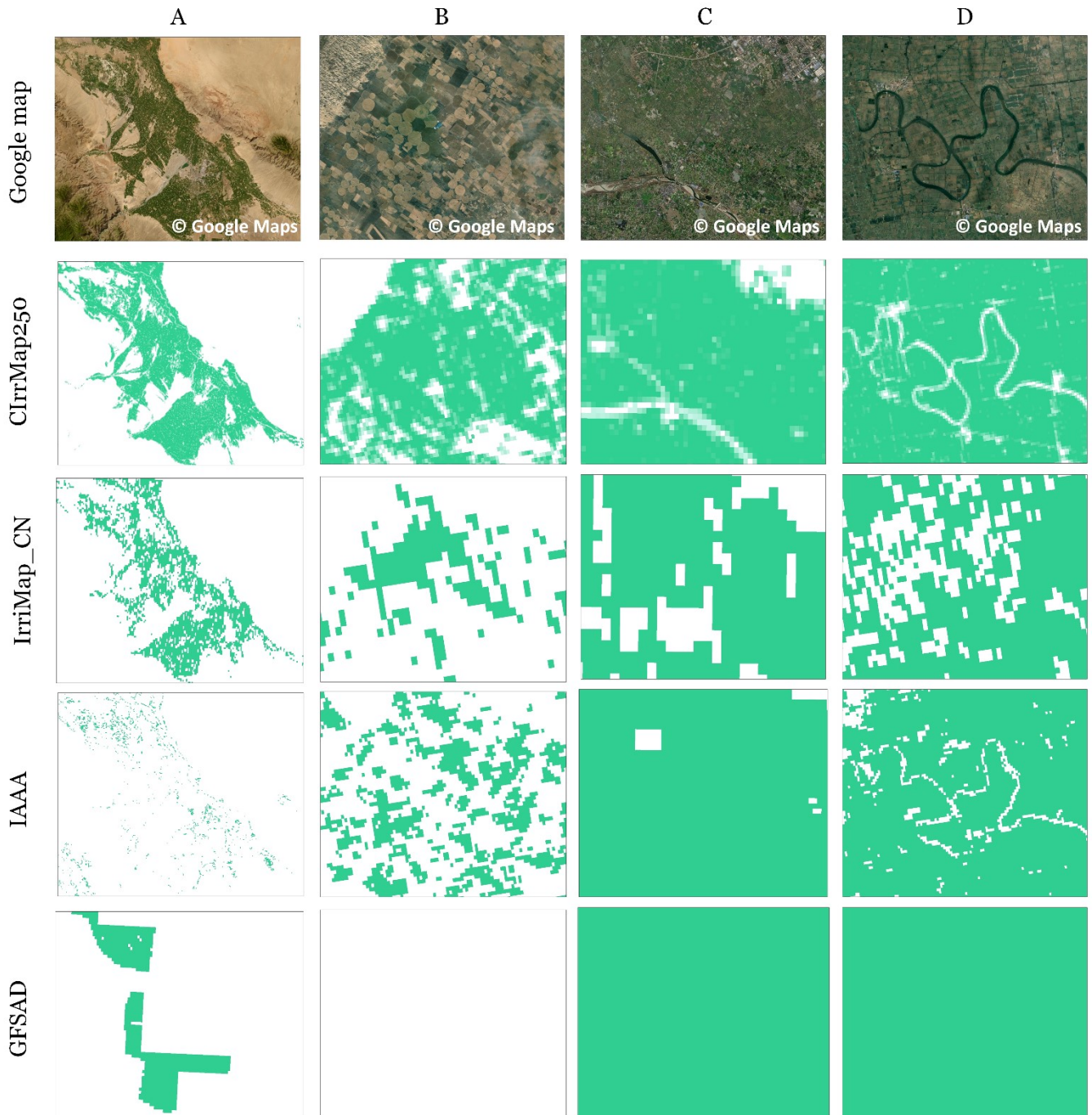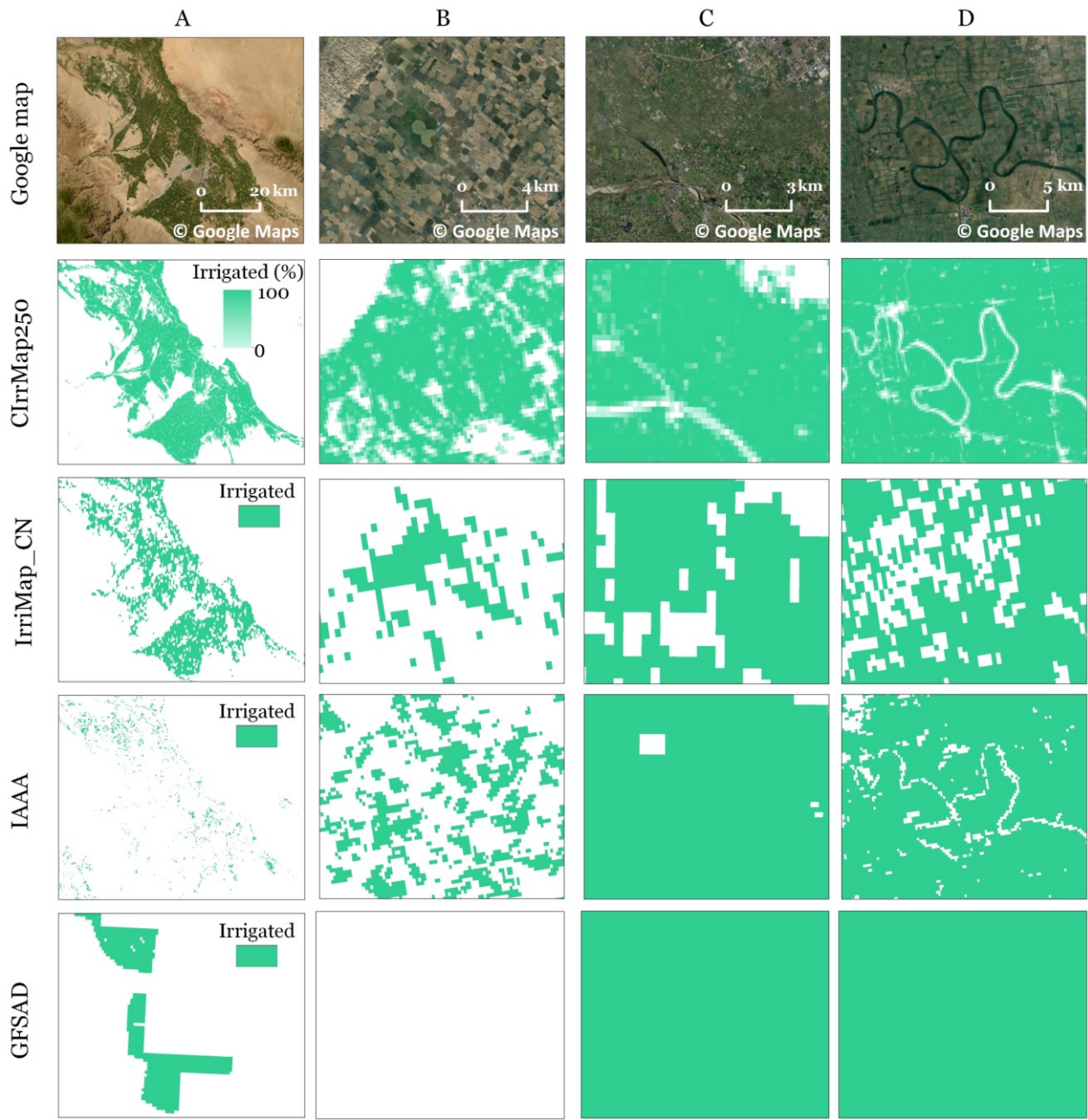
Figure 5. -**Visual comparison of CIrrMap250 with ~~the~~ existing maps.** The five rows from top to bottom correspond to the Google map, CIrrMap250, IrriMap_CN, IAAA and GFSAD, respectively. Locations of the four selected zones are presented in Figure 4a.

~~and GFSAD, respectively.~~ When examining ~~Locations of the four selected zones are presented in Figure 4a.~~

Figure 6 provides an additional comparison of the aforementioned large-scale irrigation maps with the field-scale remote sensing irrigation map (OPTRAM30) in the Hexi Corridor ~~of Northwest China.~~(Figure 6), CIrrMap250 exhibits a ~~robust~~high agreement with OPTRAM30 ~~in mapping irrigated cropland.~~. While IrriMap_CN captures the general ~~pattern of irrigated cropland~~patterns, it tends to underestimate the overall irrigation extent ~~of irrigated cropland in this~~, as demonstrated in zones I and II of the region~~. In contrast,~~ (Figure 6d). The IAAA product struggles to identify irrigated cropland in this area, displaying significant omission and commission errors. Similarly, GFSAD has a limited ability to accurately depict irrigated areas in the Hexi Corridor.
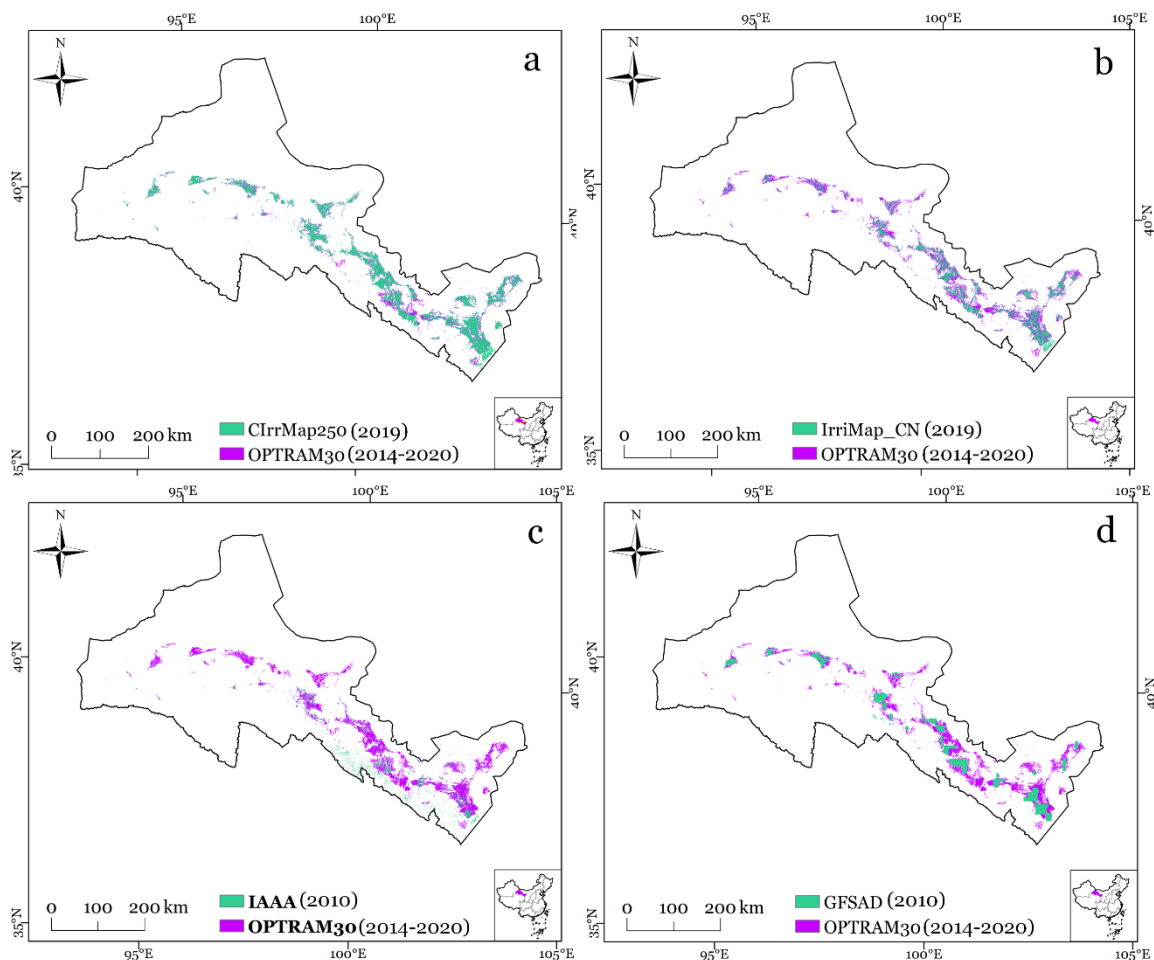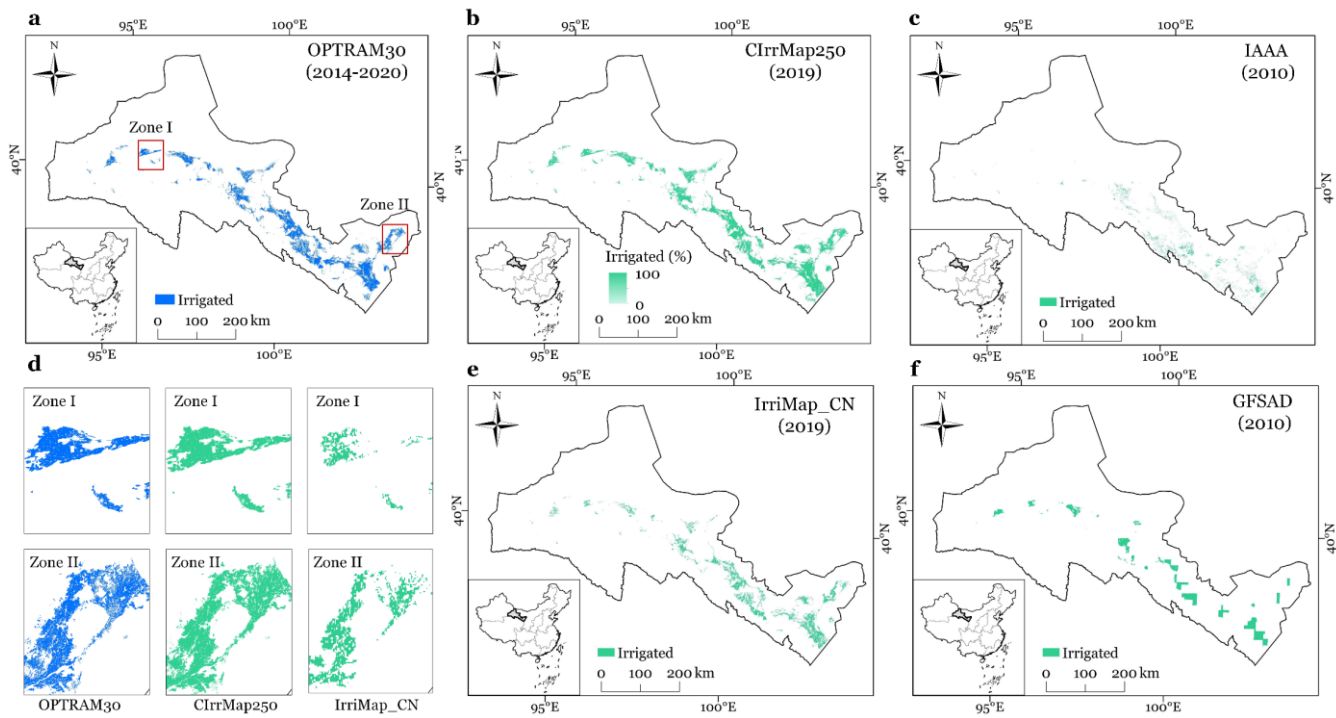
Figure 6. Comparison of large-scale irrigation maps ~~(CIrrMap250, IrriMap_CN, IAAA, GFSAD)~~ with the field-scale remote sensing irrigation map (OPTRAM30) in the Hexi Corridor of Northwest China. Panels **a**, **b**, **c**, **e**, and **f** depict the distribution of

~~4.1.3 Comparison~~ irrigated ~~area~~ cropland in OPTRAM30, CIrrMap250, IAAA, IrriMap_CN, and GFSAD, respectively. Panel **d** shows the comparisons of CIrrMap250 and IrriMap_CN with OPTRAM30 in two local zones.

4.1.3 Comparison ~~high-resolution~~with irrigation water use data

As illustrated in Figure 7, ~~there is a good correlation between the~~ the CIrrMap250-estimated ~~irrigated area and the~~ irrigation ~~water withdrawal. Changes in irrigated area determined by~~ areas exhibit a notable correlation with irrigation water withdrawals. Irrigation area changes derived from CIrrMap250 account for approximately 50% and 60% of the variance in irrigation water withdrawals ~~for the years~~ circa 2010 and 2020, respectively. In contrast, ~~changes~~variations in irrigated ~~areas derived~~area obtained from IrriMap_CN can only explain 40% and 48% of the variance in irrigation water withdrawals for ~~the same periods, namely~~ 2010 and 2020~~. The~~ , respectively. As shown in Figures 7c and f, the irrigated area estimates ~~of irrigated areas~~ from the other two maps~~, namely~~ (i.e., IAAA and GFSAD~~, are able to explain~~) demonstrate limited explanatory power, explaining only ~~a small proportion~~12% and 20% of the ~~variances~~variation in irrigation ~~water~~ withdrawals (i.e., 0.12 and 0.20), suggesting

a relatively low performance of these maps in China~~for the year 2010~~. These results indirectly imply ~~the better~~a superior performance of CIrrMap250 over ~~the~~existing ~~irrigation~~maps.
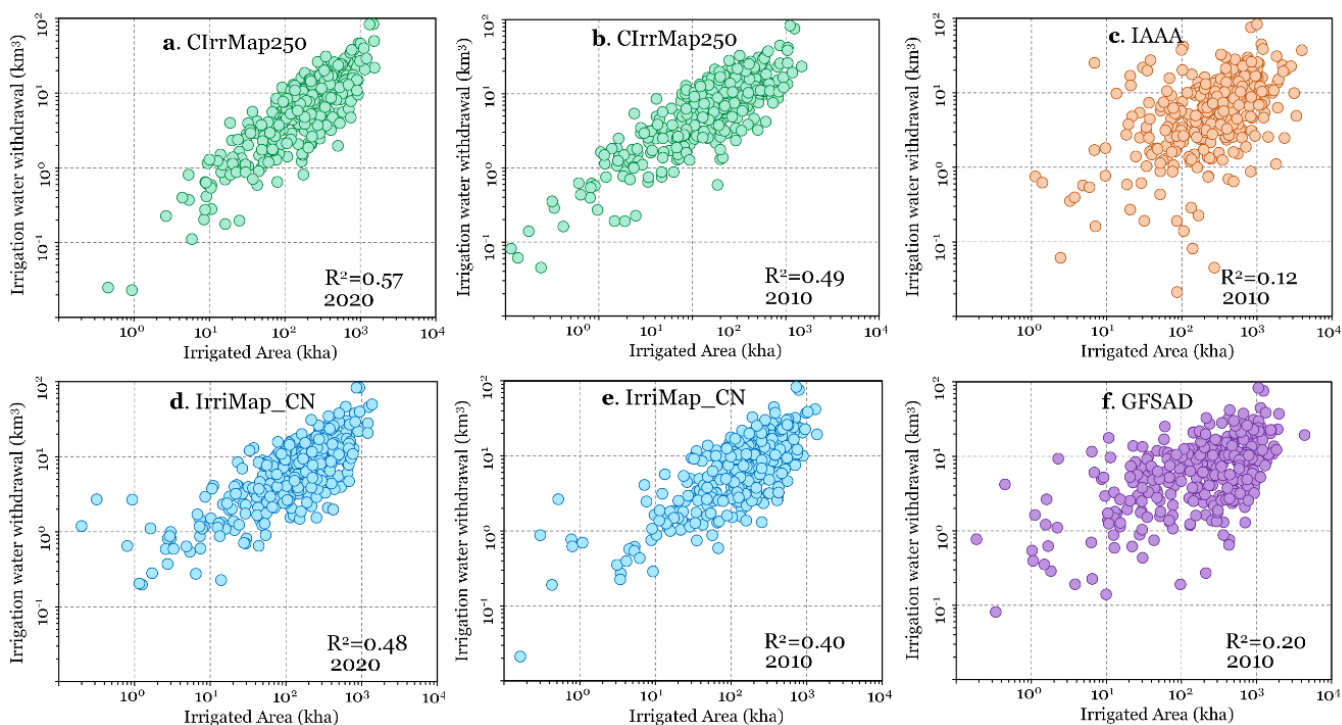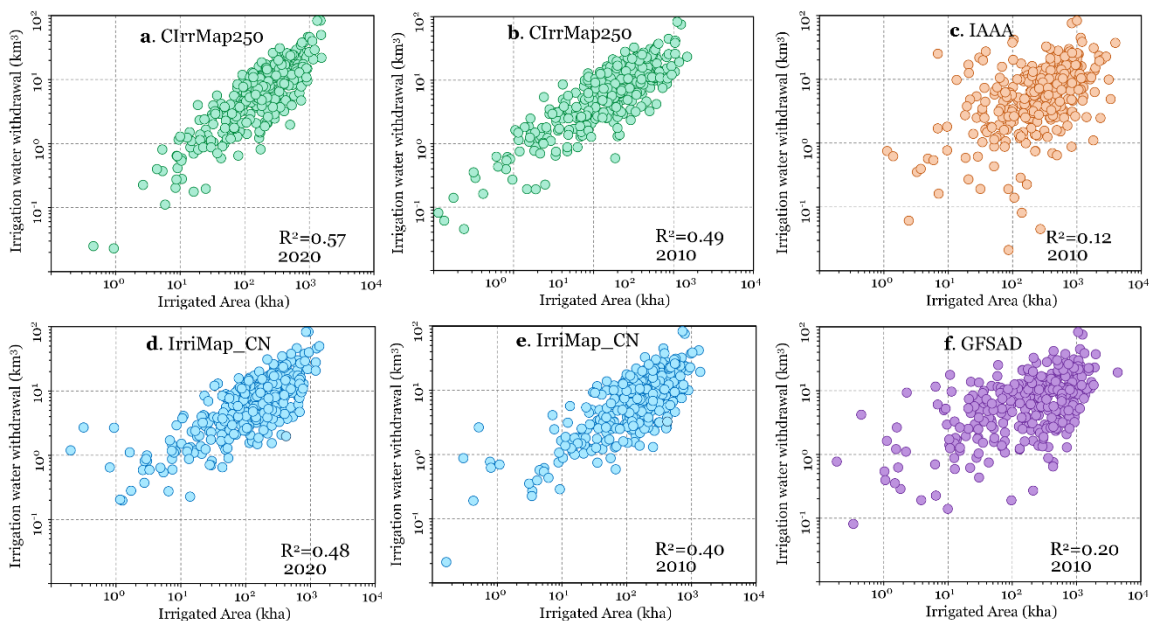
Figure 7. Scatterplots of ~~irrigated area estimates against~~ **irrigation water withdrawals against irrigated area estimates from different products for the years circa 2010 and 2020.**~~-~~ The data are presented in logarithmic units to reflect both small and large values.

4.2 Spatiotemporal changes of irrigated croplands

As depicted in Figure 8, ~~irrigated~~ our CIrrMap250 revealed that irrigation area ~~expands~~expanded significantly in NEC and NWC from 2000 to 2020. Conversely, ~~it reduced notably~~notable decreases in irrigated areas were identified in the northern parts of SC and CSC, the northeastern part of SWC, and the southern parts of CSC and NC. The decline in irrigated areas ~~tends~~tended to be concentrated in populous areas, ~~which can be~~ attributed to the rapid urban expansion on ~~large areas of~~ cropland (Zhang et al., 2024). The gravity center of ~~gravity for irrigated area is~~irrigation was situated on the border of NC and CSC, and ~~exhibits~~exhibited a noticeable northward shift ~~from 2000 to 2020.~~during the study period. This northward ~~spatial~~ trend ~~in irrigated area~~ is likely to exacerbate the water crisis in Northern China (Li et al., 2023), which has only 20% of China's water resources but supports more than half of its population. The gravity center showed clear trends in NWC, NEC, and NC but was insignificant in the remaining subregions (Supplementary Figure S5). In NWC, irrigation significantly shifted to the northwest, while in NEC, it significantly shifted to the northeast. Meanwhile, there was a northward spatial trend in irrigation in NC.
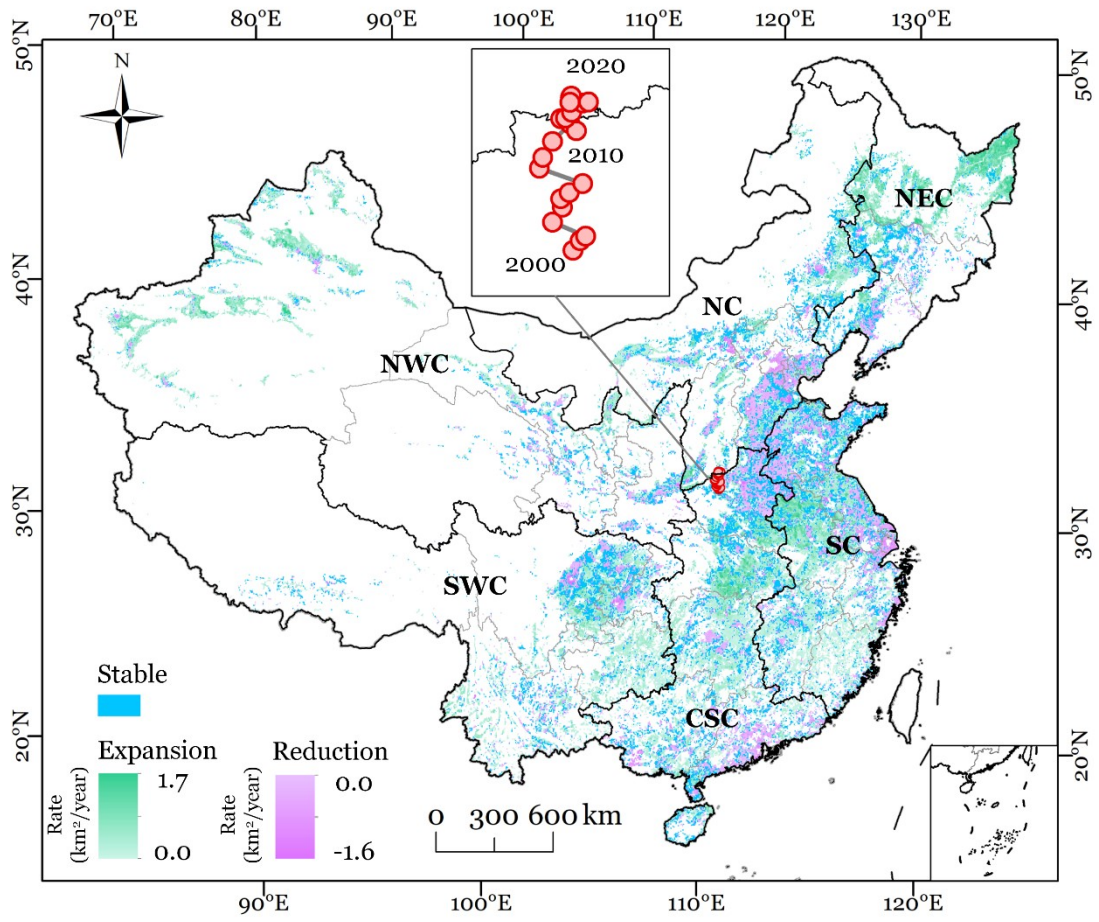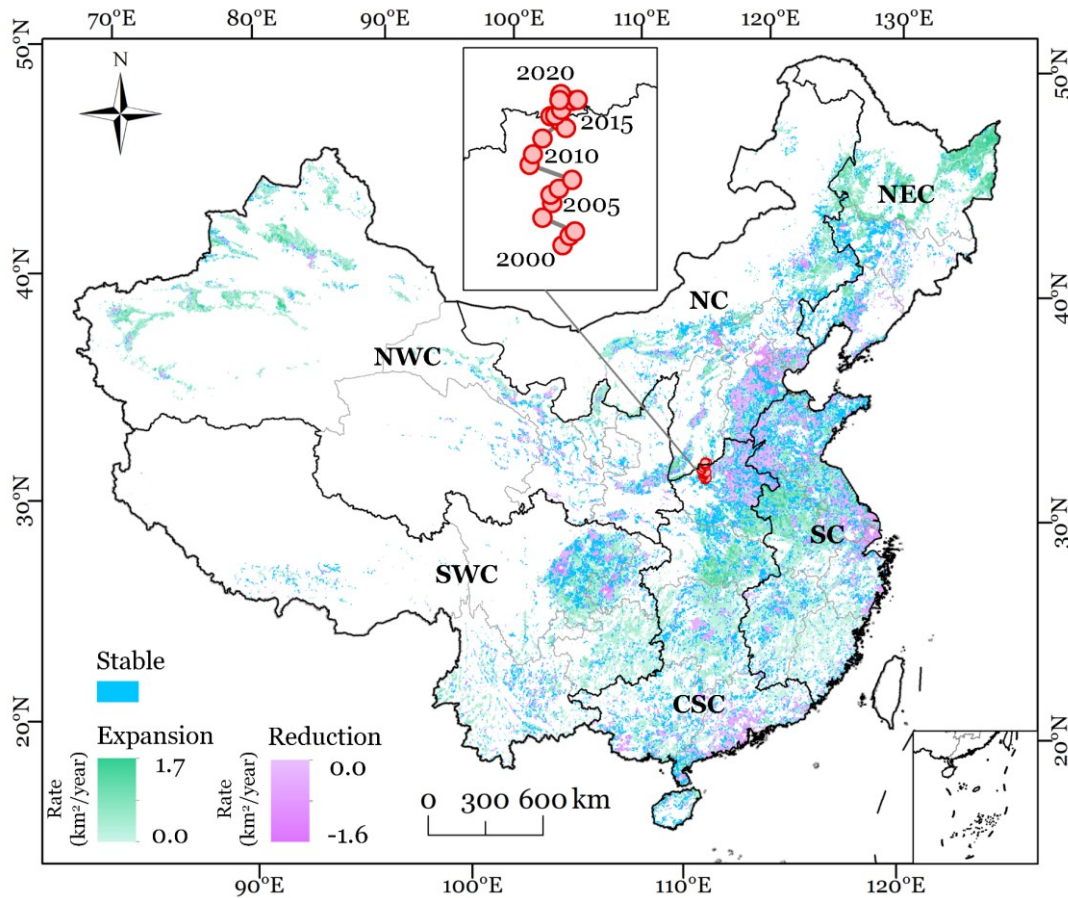
Figure 8. Spatiotemporal changes in irrigated area from 2000 to 2020. Pixels ~~with~~exhibiting significant ~~increasing or decreasing trend~~interannual trends (p~~<~~ < 0.05) ~~marked~~in irrigated area were labelled as "expansion" or "reduction", while those with insignificant changes are denoted as "stable". Pixels with ~~<~~less than 5% irrigated croplands were excluded from the map. ~~Inserted~~The inset panel on the top of the figure depicts the center-of-gravity movement (spatial trend) of China's irrigated ~~area~~areas at the national scale.

As shown in Figure 9, our annual irrigation maps indicated that all subregions ~~exhibit~~exhibited an increasing trend in irrigated area from 2000 to 2020, with NEC expanding significantly faster than the other subregions. ~~The irrigated area of China increases~~More specifically, China's irrigation aera increased from ~~750~~about 760,000 to ~~950~~940,000 km² at ~~the~~an annual rate of ~~about~~ 10,000 km²~~/year~~ (or 1.29%/year). ~~Notably, NEC and NWC contribute to about half of this expansion.~~ Despite the ~~consistent~~overall upward trend ~~in irrigated area, the relative~~, changes in the proportion of irrigated ~~areas, in relation to China's total irrigated area, are inconsistent across different subregions. The proportion of irrigated area in NEC~~ area varied by subregion - upward trends in NEC and NWC ~~and~~ ~~NWC shows an upward trend, whereas that~~decreasing in SCS, SC, and NC~~ displays a downward trend.~~. SC ~~has~~accounted for the largest proportion of irrigated cropland in China (26%-~~30~~29%), followed by CSC (22%-24%), NC (16%-17%), NWC (12%-14%), SWC (11%), and NEC (7%-11%).
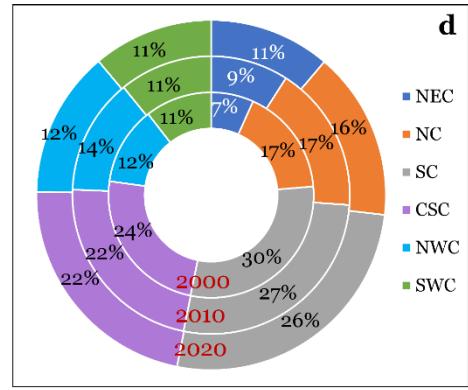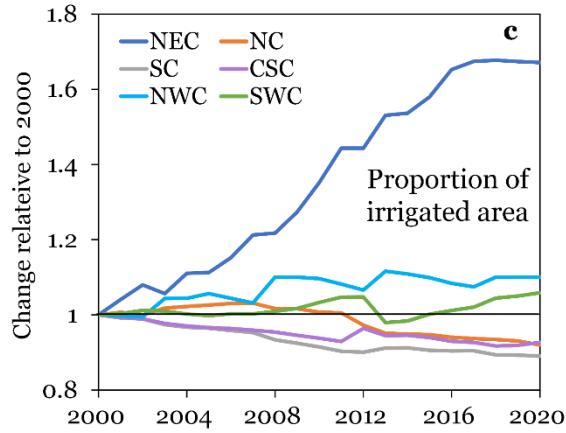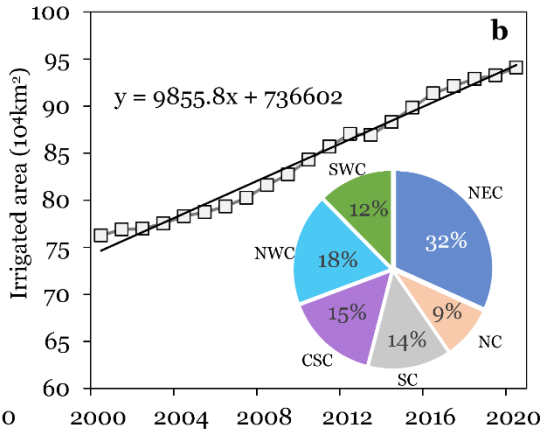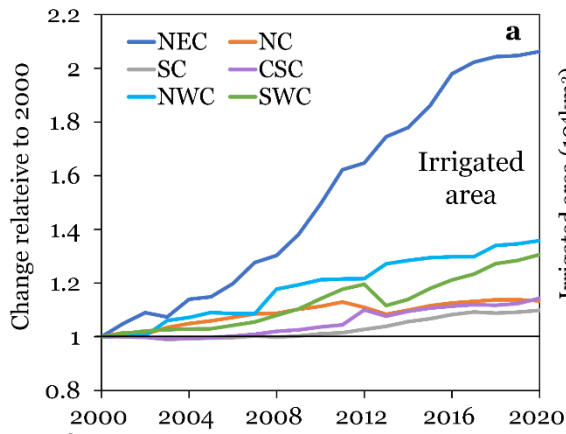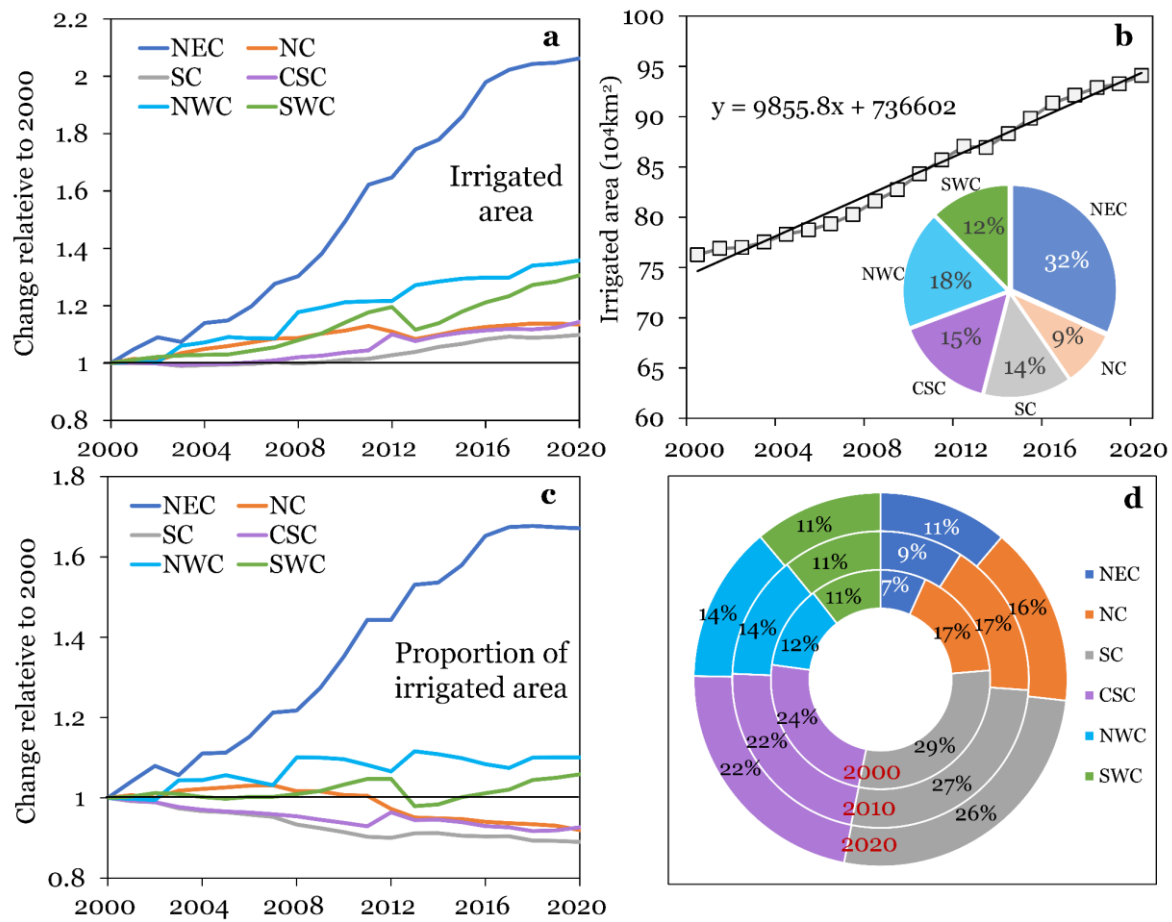
Figure 9. Changes in irrigated area ~~of~~across the six subregions of China during 2000-2020. a, Relative changes in irrigated area. **b**, Changes in China's total irrigated area, with the contribution of different subregions depicted in the inserted pie chart. **c**, Relative changes in ~~the~~ proportion of irrigated area. **d**, Proportion of irrigated area for the years 2000, 2010 and 2020.

4.3. ~~Irrigated cropland~~Irrigation changes under different water stress levels

Figure 10 shows ~~the~~irrigation changes ~~in irrigated cropland~~ under different ~~levels of~~ water stress _levels_. We ~~find~~found a gross _irrigation_ expansion of ~~irrigated area by about~~ ~250,000 km² in China from 2000 to 2020, of which 64% ~~is~~was unsustainable from the perspective of water resources and ~~has been~~was in regions with ~~high to~~ severe _to extreme_ water stress. The expansion of irrigated area ~~is~~was mainly situated in NWC, NEC, NC, and the northern parts of CSC and SC. The gross reduction ~~in irrigated area is~~was about 70,000 km², of which 72% ~~has been sustainable and located~~was in regions with ~~high to~~ severe _to extreme_ water stress~~.~~ ~~These~~ _and could be considered as sustainable. This_ sustainable reduction ~~in irrigated area,~~was primarily located in NC, CSC and SC~~, mitigates~~ _that partly mitigated_ the unstainable ~~irrigated cropland~~ expansion~~.~~ _in the regions._ The

net expansion of irrigated area ~~is~~was about 180,000 km², of which 61% ~~is~~was water unsustainable. The subregions NEC and NWC ~~have~~had a larger proportion of unsustainably expanded irrigated area compared to other subregions, accounting for about 70% of China's net unsustainable irrigation expansion. In contrast, the subregions CSC and SWC have a greater proportion of

565 ~~sustainably expanded irrigated area~~sustainable expansion than in other subregions due to the abundance of water resources and lower water stress there.
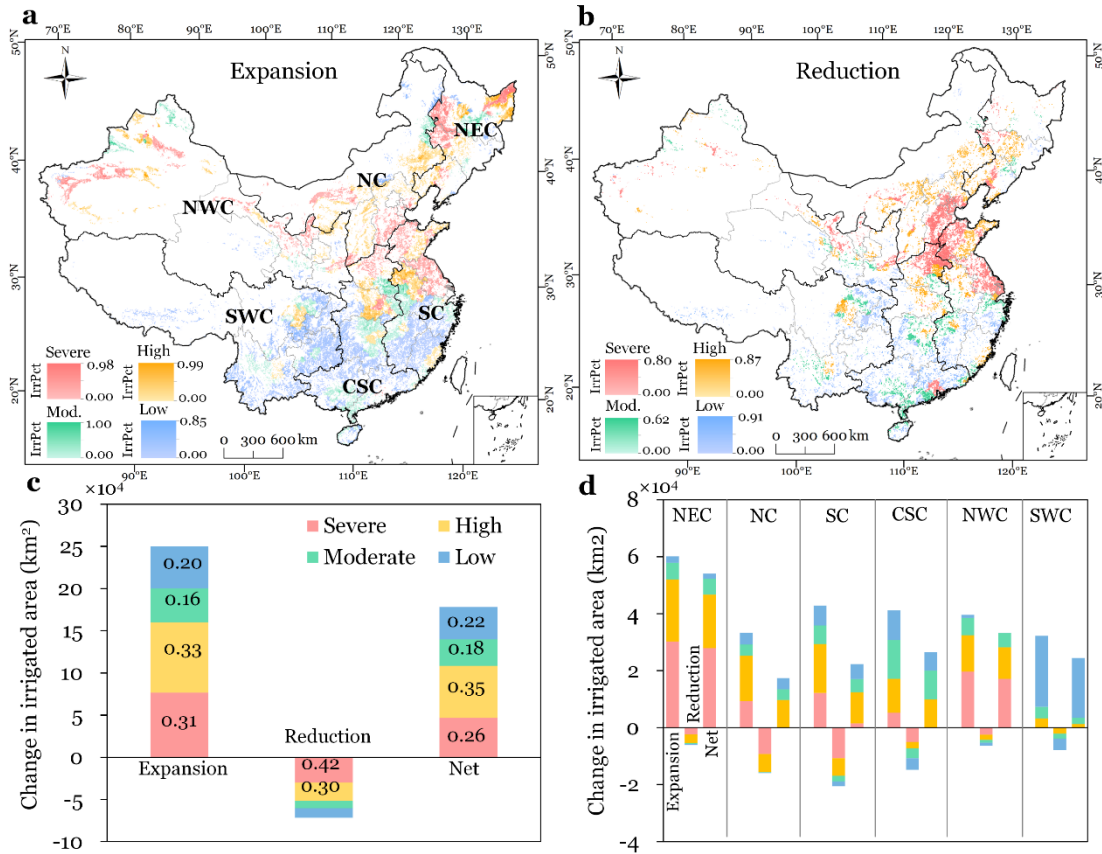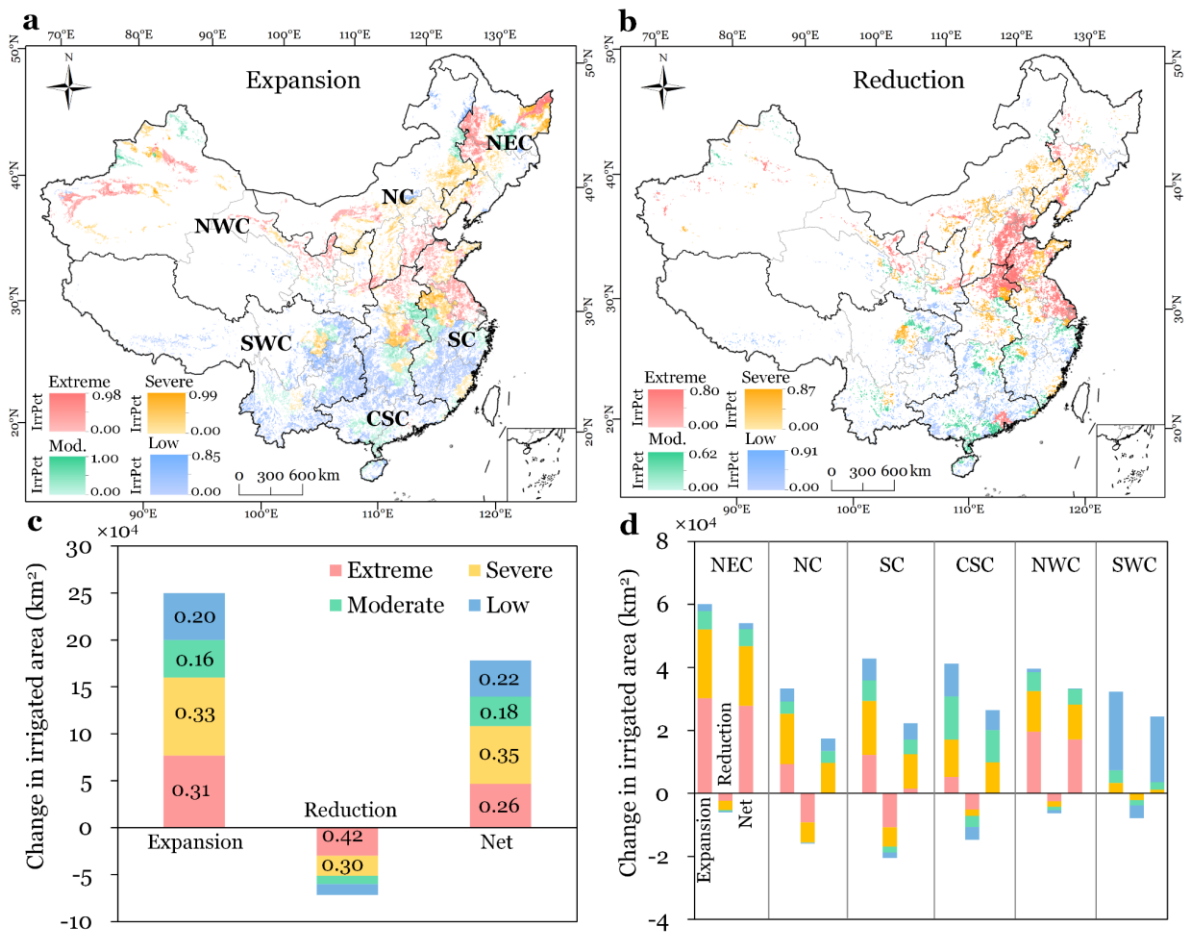
Figure 10. Changes in irrigated area between 2000 and 2020 under different water stress levels. Panels **a** and **b** show~~present~~ the spatial distribution of gross ~~expansion~~expansions and ~~reduction of~~reductions in irrigated ~~areas, respectively,~~area under ~~low to severe~~ four categories of water stress~~.~~ (i.e., low, moderate, severe, and extreme). Panel **c** ~~and d~~ show~~shows~~ the gross and net changes in irrigated area by water stress category for China~~and~~, while panel d presents the results for the six subregions.

5 Discussion

5.1 Improvement of CIrrMap250 over existing products

Our CIrrMap250 product provides annual maps of China's irrigated cropland from 2000 to 2020, exhibiting higher accuracy compared to existing products. The improved performance of CIrrMap250 can be attributed to several key factors. First,

CIrrMap250 has digested unprecedentedly detailed ~~irrigated area~~irrigation statistics and reliable national land surveys, and

580   ~~meanwhile~~at the same time, has ~~considered discrepancy been~~reconciled the discrepancies between statistical/survey data and remote sensing data. We compiled county-level statistical data for ~~over~~ 80% of provinces in China, along with prefecture-level data for the remaining provinces. These datasets, for the first time, were harmonized with ~~the national land surveys~~China's National Land Surveys, greatly reducing the errors and uncertainties in ~~irrigated area~~reported statistics. The harmonized irrigated area data were further adjusted to reconcile the statistical/~~surveyed data with remote sensing data. The reconciliation~~

585   ~~was necessary because statistical and surveyed irrigated area represents the net extent of irrigated cropland, whereas remote~~ ~~sensing-derived irrigated area indicates the gross extent. Without adjusting the original irrigated area statistics~~survey data with remote sensing data to account for their inconsistency. Without data harmonization and reconciliation, the irrigation extent would be significantly underestimated, leading to a decrease in irrigation mapping accuracy by 8%-26% (Supplementary Figure ~~S4~~S6).

590   Furthermore, CIrrMap250 ~~describes irrigated cropland distribution through~~ considered the fractional coverage of cropland within coarse-resolution pixels, rather than ~~the~~using binary ~~approach adopted~~ cropland masks in most existing products. The majority of farms in China are small and fragmented. ~~For instance, in the year 2020, we~~We observed that ~~about~~ 37% of ~~the 250-m~~China's cropland grids ~~were occupied by less than half of croplands in China, while less than~~had cropland proportions below 50% for the year 2020, and only 40% of cropland grids ~~were occupied by more than 90% of~~

595   ~~croplands.~~showed cropland proportions above 90%. Therefore, it becomes crucial to consider the fraction coverage of cropland in cropland masks for ~~the purpose of~~irrigation mapping ~~irrigated areas. We~~. To underscore this necessity, we conducted an additional ~~irrigation mapping~~ experiment, ~~in which~~wherein we adopted the 250- m cropland ~~maps were~~masks that described cropland distribution in a binary manner ~~and resampled from the 30-m hybrid cropland product.~~(i.e., each pixel was classified as either cropland or non-cropland) for irrigation mapping. As depicted in Supplementary Figure ~~S5~~S7, a substantial portion

600   of irrigated cropland would be overlooked if the fractional coverage of cropland ~~is not taken into account~~were removed, particularly in South China. The accuracy of the ~~irrigated cropland map~~final irrigation maps would decrease by approximately 5%-6% if we used such binary cropland masks (Supplementary Figure ~~S6~~S8).

Lastly, CIrrMap250 has incorporated an irrigation suitability ~~map, derived by combining irrigation suitability values~~ ~~of three influential factors elevation, slope,~~analysis, based on the premise that irrigated cropland should not only be greener

605   and ~~aridity index – using a weighted average method.~~more productive but also more suitable for irrigation compared to rainfed cropland. To demonstrate the importance of integrating irrigation suitability into the irrigation mapping process, we randomly generated 250 sets of weights (assigned to the influencing factors) for all provinces in China, resulting in 250 distinct irrigation suitability maps. Based on these maps, we then created 250 different irrigated cropland maps for the year 2010 using the method proposed ~~method of~~in this study. As shown in Supplementary Figure ~~S7~~S9, regardless of the choice of irrigation

610   suitability maps, these irrigation maps consistently outperform the baseline irrigation map, which ~~was created using the method~~ ~~in this study but excluded~~disregarded irrigation suitability during the mapping process. Furthermore, there is a narrow range

(0.75-0.77) in the overall accuracy of these irrigation maps, implying the robustness (low sensitivity) of the mapping method to the use of different irrigation suitability maps.

5.2 Uncertainties ~~and~~, limitations, and potential applications of CIrrMap250

Despite the advancements ~~made in~~of CIrrMap250 compared to existing products, we acknowledge several uncertainties and limitations associated with the product. CIrrMap250 was developed by integrating data from multiple sources using a semi-automatic training method, leveraging joint information related to irrigation in each data source. However, each data source inherently presents uncertainties and deficiencies (Shahriar Pervez et al., 2014; Tian et al., 2024)~~Firstly, the accuracy of CIrrMap250 is intricately tied to irrigated~~. Irrigation area statistics. ~~Despite our efforts to harmonize irrigation statistics with national land surveys, inherent biases and uncertainties persist~~, in particular, can contain significant uncertainties due to technical and political factors, such as variations in statistical ~~methods~~method and administrative division (Thenkabail et al., 2009; Meier et al., 2018)~~divisions.~~, which have not been well characterized. These biases and uncertainties ~~are inevitably reflected~~would manifest in CIrrMap250, since our training samples were derived from these statistics-constrained irrigation maps. In this study, we addressed this issue by merging reported irrigation statistics with independent survey results. Nonetheless, uncertainties related to irrigated areas may remain unresolved in certain regions. For instance, we found considerable discrepancies between the statistical and surveyed irrigation areas in SC and NEC (Supplementary Figure S10a), implying greater uncertainties in these subregions compared to others. Furthermore, the irrigation statistics and surveys were reconciled with remote sensing data to address inconsistencies between the two sources. However, the bias ratio may be inaccurately estimated in the reconciliation process, introducing additional uncertainties to the results.

Cropland mask layers used to distinguish cropland from non-cropland are another source of uncertainty. These layers were constructed using our hybrid cropland product (Zhang et al., 2024), which integrates five state-of-the-art remote sensing land use/cover products. This hybrid product significantly reduced uncertainties associated with cropland distribution in China. However, remote sensing-derived cropland data show large uncertainties in southern China. As illustrated in Supplementary Figure S10b, only 27% of croplands on average in SWC, SC, and CSC are consistently identified by remote sensing products, compared to 39% in northern subregions (NEC, NC, and NWC). These uncertainties are reflected in our hybrid cropland product, which shows greater accuracy in the northern subregions than in the southern ones (Supplementary Figure S10c). Meanwhile, the temporal resolution of the cropland layers is five years, which may not accurately capture changes in cropland distribution in regions experiencing rapid changes. The uncertainties and errors in the cropland mask layer, particularly in southern China, could propagate into CIrrMap250.

An additional source of uncertainty is the MODIS-derived vegetation indices (i.e., NDVI, EVI, and GI). These indices are prone to data gaps due to cloud and cloud shadow contaminations. In this study, we filled the data gaps by using a simple nearest neighbor interpolation method, which may introduce uncertainties to CIrrMap250. Additionally, irrigated croplands in humid southern China are more sparsely distributed and show weaker contrast with rainfed fields compared to northern China.

645 This makes the peak vegetation indices less effective and more uncertain in distinguishing irrigated from rainfed cropland (Xie et al., 2019; Zhang et al., 2022a)~~the statistics constrained irrigation maps. Furthermore,~~. Consequently, our CIrrMap250 product exhibits higher accuracy in NEC, NWC, and NC than in SC, CSC, and SWC subregions (Supplementary Figure S10d).

Lastly, CIrrMap250 has the limitation of a relatively coarse spatial resolution of 250 ~~meters.~~m and does not fully address the mixed-pixel problem. While ~~the~~ CIrrMap250 offers a higher spatial resolution ~~of CIrrMap250 is higher~~ than many

650 existing large-scale irrigation maps, it may ~~still not be applicable to smaller spatial scales (e.g.,~~not be suitable for local applications, such as field or irrigation district levels. The mixed-pixel problem significantly affects the precision of cropland masks (Zhang et al., 2024)~~scales). In addition, the mix-pixel problems could bring uncertainties to our mapping results. Despite the consideration of~~ and weakens the distinction between vegetation indices for irrigated and rainfed cropland. Even though CIrrMap250 considers the fractional ~~average~~coverage of cropland, ~~CIrrMap250 cannot~~it does not differentiate between

655 irrigated and ~~rain fed~~rainfed croplands at ~~the~~ subpixel scales~~.~~, like many other existing irrigation maps. There are many small and fragmented croplands in the mountainous regions of ~~South China with complex terrain and diverse vegetation types.~~southern China. CIrrMap250 should be used with caution in these ~~regions~~areas due to the ~~wide existence~~prevalence of ~~the~~ mixed pixels. ~~The mix-pixel problems could not only significantly affect the precision of cropland masks , but also the difference in vegetation indices between irrigated and rainfed cropland.~~

660 Despite these limitations, ~~our~~ CIrrMap250 makes a valuable contribution to the field of irrigation mapping and ~~will greatly~~is poised to significantly support ~~hydrologic,~~agricultural, hydrological, and climate studies, as well as water resource management in China. ~~Efforts~~Ongoing efforts to ~~overcome the above~~address these limitations and explore ~~avenues for~~ potential enhancements will undoubtedly improve the accuracy and utility of our irrigation maps in the future. One of the major applications of CIrrMap250 will be estimating irrigation water use or requirements, considering that irrigated area is a

665 dominate driver of irrigation water withdrawal (Ozdogan and Gutman, 2008; Puy et al., 2021). Secondly, the spatial detail provided by CIrrMap250 can be integrated into crop, hydrological, and climate models to improve the simulations of water uses and land-atmosphere interactions (Uniyal and Dietrich, 2021; Mcdermid et al., 2023; Yang et al., 2023). This integration will advance our understanding of how irrigation practices influence crop yield, and hydrological and climatic processes from local to nationwide scales. Lastly, CIrrMap250 provides insights into irrigation changes and can assist in optimizing the spatial

670 distribution of irrigated croplands (Rosa et al., 2020a; Rosa et al., 2020b), thereby supporting more informed decisions for sustainable water and land use.

6 Data availability

The annual maps of China's irrigated cropland from 2000 to 2020 (named as CIrrMap250) can be accessed at:

675 https://doi.org/10.6084/m9.figshare.24814293.v1 (Zhang et al., 2023a). All maps are presented in the GeoTIFF format, with the geographic ~~coordinates using the~~coordinate of WGS84 ~~reference system.~~. Pixel size is 0.00225 × 0.00225 degree (~250 m

×250 m at Equator). ~~The maps show the percentage of each 250 m pixel that is covered by irrigated cropland (i.e., pixel value = irrigated area / pixel area ×100).~~

680 7 Conclusions

~~This study outlines the development of~~ China, as a big agricultural country with extensive irrigation, underscores the critical importance of developing reliable irrigation maps for sustainable land-water-food nexus management. This study presented new annual maps of irrigated cropland in China spanning from 2000 to 2020, ~~denoted~~referred to as CIrrMap250. ~~The new product was~~These maps were developed by integrating multisource data, including remote sensing data ~~(vegetation indices,~~
685 ~~hybrid cropland product, and paddy field maps), irrigated area~~, reported statistics and surveys, and an irrigation suitability map. ~~The integration of these data was achieved through a semi-automatic training approach, which first generated training samples using a threshold calibration method and subsequently employed the random forest algorithm for classifying irrigated and rainfed cropland. We evaluated the accuracy of CIrrMap250 using over~~ Validation against 20,~~000~~720 reference ~~collected from existing literatures and land use maps of the National Land Survey in China. Furthermore, an indirect assessment of~~
690 ~~CIrrMap250 was carried out using higher resolution data on irrigation water withdrawals. Our CIrrMap250 product was compared to three available large-scale~~ samples demonstrated that our irrigation maps ~~(i.e., IrriMap_CN, IAAA, and GFSAD) as well as a field-scale map (i.e., OPTRAM30).~~

~~Results indicated that CIrrMap250 attained an overall accuracy of 0.79-0.88 for the years 2000, 2010 and 2020, surpassing the precision of the existing~~ achieved high accuracy and outperformed the currently available products~~.~~
695 ~~Furthermore, the CIrrMap250-estimated irrigated area can explain 50-60% of the variance in prefecture-level irrigation water withdrawals, and showed a stronger correlation with irrigation water withdrawals than the existing products. The visual comparison~~ covering the entire China. The superiority of our product over existing maps were further confirmed ~~the better performance of CIrrMap250 over the existing products. Leveraging~~through the assessments using irrigation water withdrawal data and local-scale visual comparisons. Based on the 21 years of data, we found a ~~consistent~~clear upward trend ~~in the irrigated~~
700 ~~area across all subregions of China from 2000 to 2020. Notably, the growth rate in Northeast and Northwest China surpasses that of the remaining subregions. Consequently, the center of gravity of China's irrigated cropland shifted significantly~~and northward shift in China's irrigation area. The irrigation expansion is particular notable in water-scare regions like Northeast China and Northwest China, potentially exacerbating ~~the~~ water ~~crisis in North China. Over the period from 2000 to 2020, we observed a net increase of about 180,000 km² (or 25%) in China's irrigated area. However, a significant portion (61%) of this~~
705 ~~expansion is deemed unsustainable from a water resources perspective and have been in regions facing high to severe water stress.~~

~~The performance improvement of CIrrMap250 over existing products can be attributed to the digestion of detailed irrigated area statistics and reliable national land surveys, the consideration of discrepancy been statistical/survey data and~~

710 remote sensing data, the description of irrigation cropland distribution through fractional coverage, and the incorporation of irrigation suitability. We anticipate that our CIrrMap250 product scarcity concerns. CIrrMap250 will greatly support hydrologic,significantly enhance agricultural, hydrological, and climate studies, as well as water resource management in China for improved water and land resources management. .

Author contribution

715 LZ conceived the research, carried out the experiments, analysed the results, and prepared the manuscript with contributions from all co-authors. YX analysed the results, provided the technical support, reviewed and edited the manuscript. XZ and QM collected the validation dataset. LB reviewed and edited the manuscript, and supervised the work.

Competing interests

The authors declare that they have no conflict of interest.

720 ## Acknowledgements

This study is supported by the National Natural Science Foundation of China (42271286 and 41901045), and), the Youth Innovation Promotion Association of Chinese Academy of Sciences (2023454), and Key Research Program of Gansu Province (Grant No. 23ZDKA0004). We greatly appreciate the Ministry of Natural Resource of the People's Republic of China for the data provision.

725

References

Ambika, A. K., Wardlow, B., and Mishra, V.: Remotely sensed high resolution irrigated area mapping in India for 2000 to 2015, Scientific Data, 3, 160118, 10.1038/sdata.2016.118, 2016.

Bai, M., Zhou, S., and Tang, T.: A Reconstruction of Irrigated Cropland Extent in China from 2000 to 2019 Using the Synergy
730 of Statistics and Satellite-Based Datasets, Land, 11, 1686, 10.3390/land11101686, 2022.

Bhattarai, N., Lobell, D. B., Balwinder, S., Fishman, R., Kustas, W. P., Pokhrel, Y., and Jain, M.: Warming temperatures exacerbate groundwater depletion rates in India, Science Advance, 9, eadi1401, 10.1126/sciadv.adi1401, 2023.

Breiman, L.: Random Forests, Machine Learning, 45, 5-32, 10.1023/A:1010933404324, 2001.

Chen, F., Zhao, H., Roberts, D., Van de Voorde, T., Batelaan, O., Fan, T., and Xu, W.: Mapping center pivot irrigation systems
735 in global arid regions using instance segmentation and analyzing their spatial relationship with freshwater resources,

Remote Sensing of Environment, 297, 113760, 10.1016/j.rse.2023.113760, 2023.

Chen, X., Yu, L., Du, Z., Liu, Z., Qi, Y., Liu, T., and Gong, P.: Toward sustainable land use in China: A perspective on China's national land surveys, Land Use Policy, 123, 106428, 10.1016/j.landusepol.2022.106428, 2022.

Cheng, G., Li, X., Zhao, W., Xu, Z., Feng, Q., Xiao, S., and Xiao, H.: Integrated study of the water–ecosystem–economy in the Heihe River Basin, National Science Review, 1, 413-428, 2014.

Dari, J., Quintana-Seguí, P., José Escorihuela, M., Stefan, V., Brocca, L., and Morbidelli, R.: Detecting and mapping irrigated areas in a Mediterranean environment by using remote sensing soil moisture and a land surface model, Journal of Hydrology, 596, 126129, https://doi.org/10.1016/j.jhydrol.2021.126129, 2021.

Debeurs, K. and Townsend, P.: Estimating the effect of gypsy moth defoliation using MODIS, Remote Sensing of Environment, 112, 3983-3990, 10.1016/j.rse.2008.07.008, 2008.

Deines, J. M., Kendall, A. D., and Hyndman, D. W.: Annual Irrigation Dynamics in the U.S. Northern High Plains Derived from Landsat Satellite Data, Geophysical Research Letters, 44, 9350-9360, 10.1002/2017GL074071, 2017.

Deines, J. M., Kendall, A. D., Crowley, M. A., Rapp, J., Cardille, J. A., and Hyndman, D. W.: Mapping three decades of annual irrigation across the US High Plains Aquifer using Landsat and Google Earth Engine, Remote Sensing of Environment, 233, 111400, 10.1016/j.rse.2019.111400, 2019.

Elwan, E., Le Page, M., Jarlan, L., Baghdadi, N., Brocca, L., Modanesi, S., Dari, J., Quintana Seguí, P., and Zribi, M.: Irrigation Mapping on Two Contrasted Climatic Contexts Using Sentinel-1 and Sentinel-2 Data, 2022.

Esmaeili, P., Vazifedoust, M., Rahmani, M., and Pakdel, H.: A simple rule-based algorithm in Google Earth Engine for operational discrimination of rice paddies in Sefidroud Irrigation Network, Arabian Journal of Geosciences, 16, 649, 10.1007/s12517-023-11770-x, 2023.

Gao, B.-c.: NDWI—A normalized difference water index for remote sensing of vegetation liquid water from space, Remote Sensing of Environment, 58, 257-266, https://doi.org/10.1016/S0034-4257(96)00067-3, 1996.

Gao, Q., Zribi, M., Escorihuela, M., Baghdadi, N., and Segui, P.: Irrigation Mapping Using Sentinel-1 Time Series at Field Scale, Remote Sensing, 10, 1495, 10.3390/rs10091495, 2018.

Gitelson, A. A.: Remote estimation of canopy chlorophyll content in crops, Geophysical Research Letters, 32, 10.1029/2005GL022688, 2005.

Guo, Q. and Zhou, X.: Irrigated cropland expansion exacerbates the urban moist heat stress in northern India, Environmental Research Letters, 2022.

Hilker, T., Lyapustin, A. I., Tucker, C. J., Sellers, P. J., Hall, F. G., and Wang, Y.: Remote sensing of tropical ecosystems: Atmospheric correction and cloud masking matter, Remote Sensing of Environment, 127, 370-384, 10.1016/j.rse.2012.08.035, 2012.

Huete, A. R., Liu, H. Q., Batchily, K., and van Leeuwen, W.: A comparison of vegetation indices over a global set of TM images for EOS-MODIS, Remote Sensing of Environment, 59, 440-451, https://doi.org/10.1016/S0034-4257(96)00112-5, 1997.

770   International Commission on Irrigation and Drainage: World Irrigated Area-2018, https://www.icid.org/world-irrigated-area.pdf, 1-6, 2018.

Kang, S. and Eltahir, E. A. B.: North China Plain threatened by deadly heatwaves due to climate change and irrigation, Nature Communications, 9, 10.1038/s41467-018-05252-y, 2018.

Lacroix, P., Dehecq, A., and Taipe, E.: Irrigation-triggered landslides in a Peruvian desert caused by modern intensive farming, Nature Geoscience, 13, 56-60, 10.1038/s41561-019-0500-x, 2020.

Lamb, S. E., Haacker, E. M. K., and Smidt, S. J.: Influence of Irrigation Drivers Using Boosted Regression Trees: Kansas High Plains, Water Resources Research, 57: e2020WR028867, 10.1029/2020WR028867, 2021.

Li, H. and Chen, Y.: Assessing potential land suitable for surface irrigation using groundwater data and multi-criteria evaluation in Xinjiang inland river basin, Computers and Electronics in Agriculture, 168, 105079, 10.1016/j.compag.2019.105079, 2020.

Li, X., Zhang, Y., Ma, N., Zhang, X., Tian, J., Zhang, L., McVicar, T. R., Wang, E., and Xu, J.: Increased Grain Crop Production Intensifies the Water Crisis in Northern China, Earth's Future, 11, 10.1029/2023EF003608, 2023.

Liu, J., Kuang, W., Zhang, Z., Xu, X., Qin, Y., Ning, J., Zhou, W., Zhang, S., Li, R., Yan, C., Wu, S., Shi, X., Jiang, N., Yu, D., Pan, X., and Chi, W.: Spatiotemporal characteristics, patterns, and causes of land-use changes in China since the late 1980s, Journal of Geographical Sciences, 24, 195-210, 10.1007/s11442-014-1082-6, 2014.

Liu, Y., Li, Q., and Wu, W.: Analysis of feature slection for mapping irrigated cropland in northern China (In Chinese), Chinese Journal of Agricultural Resources and Regional Planning, 42, 27-35, 2022.

Longo-Minnolo, G., Consoli, S., Vanella, D., Ramírez-Cuesta, J. M., Greimeister-Pfeil, I., Neuwirth, M., and Vuolo, F.: A stand-alone remote sensing approach based on the use of the optical trapezoid model for detecting the irrigated areas, Agricultural Water Management, 274, 107975, 10.1016/j.agwat.2022.107975, 2022.

Lu, Y., Song, W., Lü, J., Chen, M., Su, Z., Zhang, X., and Li, H.: A pixel-based spectral matching method for mapping high-resolution irrigated areas using EVI time series, Remote sensing letters, 12, 169-178, 10.1080/2150704X.2020.1837987, 2021.

Massari, C., Modanesi, S., Dari, J., Gruber, A., De Lannoy, G. J. M., Girotto, M., Quintana-Seguí, P., Le Page, M., Jarlan, L., Zribi, M., Ouaadi, N., Vreugdenhil, M., Zappa, L., Dorigo, W., Wagner, W., Brombacher, J., Pelgrum, H., Jaquot, P., Freeman, V., Volden, E., Fernandez Prieto, D., Tarpanelli, A., Barbetta, S., and Brocca, L.: A Review of Irrigation Information Retrievals from Space and Their Utility for Users, Remote Sensing, 13, 4112, 10.3390/rs13204112, 2021.

McDermid, S., Nocco, M., Lawston-Parker, P., Keune, J., Pokhrel, Y., Jain, M., Jägermeyr, J., Brocca, L., Massari, C., Jones, A. D., Vahmani, P., Thiery, W., Yao, Y., Bell, A., Chen, L., Dorigo, W., Hanasaki, N., Jasechko, S., Lo, M.-H., Mahmood, R., Mishra, V., Mueller, N. D., Niyogi, D., Rabin, S. S., Sloat, L., Wada, Y., Zappa, L., Chen, F., Cook, B. I., Kim, H., Lombardozzi, D., Polcher, J., Ryu, D., Santanello, J., Satoh, Y., Seneviratne, S., Singh, D., and Yokohata, T.: Irrigation in the Earth system, Nature Reviews Earth & Environment, 10.1038/s43017-023-00438-5, 2023.

McDermid, S. S., Mahmood, R., Hayes, M. J., Bell, J. E., and Lieberman, Z.: Minimizing trade-offs for sustainable irrigation,

Nature Geoscience, 14, 706-709, 10.1038/s41561-021-00830-0, 2021.

805 McFeeters, S. K.: The use of the Normalized Difference Water Index (NDWI) in the delineation of open water features, International Journal of Remote Sensing, 17, 1425-1432, 10.1080/01431169608948714, 1996.

Mehta, P., Siebert, S., Kummu, M., Deng, Q., Ali, T., Marston, L., Xie, W., and Davis, K. F.: Half of twenty-first century global irrigation expansion has been in water-stressed regions, Nature Water, 10.1038/s44221-024-00206-9, 2024.

Meier, J., Zabel, F., and Mauser, W.: A global approach to estimate irrigated areas – a comparison between different data and

810 statistics, Hydrology and Earth System Sciences, 22, 1119-1133, 10.5194/hess-22-1119-2018, 2018.

Mishra, V., Ambika, A. K., Asoka, A., Aadhar, S., Buzan, J., Kumar, R., and Huber, M.: Moist heat stress extremes in India enhanced by irrigation, Nature Geoscience, 13, 722-728, 10.1038/s41561-020-00650-8, 2020.

Mpakairi, K. S., Dube, T., Sibanda, M., and Mutanga, O.: Fine-scale characterization of irrigated and rainfed croplands at national scale using multi-source data, random forest, and deep learning algorithms, ISPRS Journal of

815 Photogrammetry and Remote Sensing, 204, 117-130, 10.1016/j.isprsjprs.2023.09.006, 2023.

Noori, R., Maghrebi, M., Mirchi, A., Tang, Q., Bhattarai, R., Sadegh, M., Noury, M., Torabi Haghighi, A., Kløve, B., and Madani, K.: Anthropogenic depletion of Iran's aquifers, Proceedings of the National Academy of Sciences, 118, e2024221118, 10.1073/pnas.2024221118, 2021.

Ozdogan, M. and Gutman, G.: A new methodology to map irrigated areas using multi-temporal MODIS and ancillary data: An

820 application example in the continental US, Remote Sensing of Environment, 112, 3520-3537, 10.1016/j.rse.2008.04.010, 2008.

Ozdogan, M., Yang, Y., Allez, G., and Cervantes, C.: Remote Sensing of Irrigated Agriculture: Opportunities and Challenges, Remote Sensing, 2, 2274-2304, 10.3390/rs2092274, 2010.

Pervez, M. S. and Brown, J. F.: Mapping Irrigated Lands at 250-m Scale by Merging MODIS Data and National Agricultural

825 Statistics, Remote Sensing, 2, 2388-2412, 10.3390/rs2102388, 2010.

Potapov, P., Turubanova, S., Hansen, M. C., Tyukavina, A., Zalles, V., Khan, A., Song, X.-P., Pickens, A., Shen, Q., and Cortez, J.: Global maps of cropland extent and change show accelerated cropland expansion in the twenty-first century, Nature Food, 10.1038/s43016-021-00429-z, 2021.

Priestley, C. H. B. and Taylor, R. J.: On the Assessment of Surface Heat Flux and Evaporation Using Large-Scale Parameters,

830 Monthly Weather Review, 100, 81-92, 10.1175/1520-0493(1972)100<0081:OTAOSH>2.3.CO;2, 1972.

Pun, M., Mutiibwa, D., and Li, R.: Land Use Classification: A Surface Energy Balance and Vegetation Index Application to Map and Monitor Irrigated Lands, Remote Sensing, 9, 1256, 10.3390/rs9121256, 2017.

Puy, A., Borgonovo, E., Lo Piano, S., Levin, S. A., and Saltelli, A.: Irrigated areas drive irrigation water withdrawals, Nature Communications, 12, 4525, 10.1038/s41467-021-24508-8, 2021.

835 Qin, Y., Hong, C., Zhao, H., Siebert, S., Abatzoglou, J. T., Huning, L. S., Sloat, L. L., Park, S., Li, S., Munroe, D. K., Zhu, T., Davis, S. J., and Mueller, N. D.: Snowmelt risk telecouplings for irrigated agriculture, Nature Climate Change, 10.1038/s41558-022-01509-z, 2022.

Rosa, L., Chiarelli, D. D., Rulli, M. C., Dell Angelo, J., and D Odorico, P.: Global agricultural economic water scarcity, Science Advances, 6, eaaz6031, 10.1126/sciadv.aaz6031, 2020a.

840 Rosa, L., Chiarelli, D. D., Sangiorgio, M., Beltran-Peña, A. A., Rulli, M. C., D Odorico, P., and Fung, I.: Potential for sustainable irrigation expansion in a 3 °C warmer climate, Proceedings of the National Academy of Sciences, 202017796, 10.1073/pnas.2017796117, 2020b.

Rouse, J. W., Haas, R. H., Schell, J. A., and Deering, D. W.: Monitoring vegetation systems in the Great Plains with ERTS. In: Proc. Third Earth Resources Technology Satellite-1 Symposium, SP-351, Greenbelt, MD, pp. 309–317, 1974.

845 Salmon, J. M., Friedl, M. A., Frolking, S., Wisser, D., and Douglas, E. M.: Global rain-fed, irrigated, and paddy croplands: A new high resolution map derived from remote sensing, crop inventories and climate data, International Journal of Applied Earth Observation and Geoinformation, 38, 321-334, 10.1016/j.jag.2015.01.014, 2015.

Schepaschenko, D., See, L., Lesiv, M., McCallum, I., Fritz, S., Salk, C., Moltchanova, E., Perger, C., Shchepashchenko, M., Shvidenko, A., Kovalevskyi, S., Gilitukha, D., Albrecht, F., Kraxner, F., Bun, A., Maksyutov, S., Sokolov, A., Dürauer,
850 M., Obersteiner, M., Karminov, V., and Ontikov, P.: Development of a global hybrid forest mask through the synergy of remote sensing, crowdsourcing and FAO statistics, Remote Sensing of Environment, 162, 208-220, 10.1016/j.rse.2015.02.011, 2015.

Shahriar Pervez, M., Budde, M., and Rowland, J.: Mapping irrigated areas in Afghanistan over the past decade using MODIS NDVI, Remote Sensing of Environment, 149, 155-165, 10.1016/j.rse.2014.04.008, 2014.

855 Siddiqui, S., Cai, X., and Chandrasekharan, K.: Irrigated Area Map Asia and Africa. International Water Management Institute. https://waterdata.iwmi.org/applications/irri_area/, 2016.

Teluguntla, P., Thenkabail, P. S., Oliphant, A., Xiong, J., Gumma, M. K., Congalton, R. G., Yadav, K., and Huete, A.: A 30-m landsat-derived cropland extent product of Australia and China using random forest machine learning algorithm on Google Earth Engine cloud computing platform, ISPRS Journal of Photogrammetry and Remote Sensing, 144, 325-
860 340, 10.1016/j.isprsjprs.2018.07.017, 2018.

Thenkabail, P., Knox, J., Ozdogan, M., Gumma, M., Congalton, R., Wu, Z., Milesi, C., Finkral, A., Marshall, M., Mariotto, I., You, S., Giri, C., and Nagler, P.: NASA Making Earth System Data Records for Use in Research Environments (MEaSUREs) Global Food Security Support Analysis Data (GFSAD) Crop Dominance 2010 Global 1 km V001, distributed by NASA EOSDIS Land Processes Distributed Active Archive Center,
865 https://doi.org/10.5067/MEaSUREs/GFSAD/GFSAD1KCD.001. Accessed 2023-10-17., 2016.

Thenkabail, P. S., Biradar, C. M., Noojipady, P., Dheeravath, V., Li, Y., Velpuri, M., Gumma, M., Gangalakunta, O. R. P., Turral, H., Cai, X., Vithanage, J., Schull, M. A., and Dutta, R.: Global irrigated area map (GIAM), derived from remote sensing, for the end of the last millennium, International Journal of Remote Sensing, 30, 3679-3733, 10.1080/01431160802698919, 2009.

870 Thiery, W., Visser, A. J., Fischer, E. M., Hauser, M., Hirsch, A. L., Lawrence, D. M., Lejeune, Q., Davin, E. L., and Seneviratne, S. I.: Warming of hot extremes alleviated by expanding irrigation, Nature Communications, 11, 10.1038/s41467-019-

14075-4, 2020.

Thorslund, J., Bierkens, M. F. P., Oude Essink, G. H. P., Sutanudjaja, E. H., and van Vliet, M. T. H.: Common irrigation drivers of freshwater salinisation in river basins worldwide, Nature Communications, 12, 10.1038/s41467-021-24281-8, 2021.

Tian, X., Dong, J., Chen, X., Zhou, J., Gao, M., Wei, L., Kang, X., Zhao, D., Zhang, H., Crow, W. T., Huang, R., Shao, W., and Zhou, H.: County-Level Evaluation of Large-Scale Gridded Data Sets of Irrigated Area Over China, Journal of Geophysical Research: Atmospheres, 129, e2023JD040333, https://doi.org/10.1029/2023JD040333, 2024.

UNESCO World Water Assessment Programme: The United Nations world water development report 2019: leaving no one behind. Paris, UNESCO. https://unesdoc.unesco.org/ark:/48223/pf0000367306, 2019.

Uniyal, B. and Dietrich, J.: Simulation of Irrigation Demand and Control in Catchments ‡ A Review of Methods and Case Studies, Water Resources Research, n/a, e2020WR029263, https://doi.org/10.1029/2020WR029263, 2021.

Wang, C., Chen, J., Gu, L., Wu, G., Tong, S., Xiong, L., and Xu, C.-Y.: A pathway analysis method for quantifying the contributions of precipitation and potential evapotranspiration anomalies to soil moisture drought, Journal of Hydrology, 621, 129570, 10.1016/j.jhydrol.2023.129570, 2023.

Worqlul, A. W., Collick, A. S., Rossiter, D. G., Langan, S., and Steenhuis, T. S.: Assessment of surface water irrigation potential in the Ethiopian highlands: The Lake Tana Basin, Catena, 129, 76-85, 10.1016/j.catena.2015.02.020, 2015.

Worqlul, A. W., Jeong, J., Dile, Y. T., Osorio, J., Schmitter, P., Gerik, T., Srinivasan, R., and Clark, N.: Assessing potential land suitable for surface irrigation using groundwater in Ethiopia, Applied Geography, 85, 1-13, 10.1016/j.apgeog.2017.05.010, 2017.

Wu, B., Tian, F., Zhang, M., Piao, S., Zeng, H., Zhu, W., Liu, J., Elnashar, A., and Lu, Y.: Quantifying global agricultural water appropriation with data derived from earth observations, Journal of Cleaner Production, 358, 131891, 10.1016/j.jclepro.2022.131891, 2022.

Xiang, K., Yuan, W., Wang, L., and Deng, Y.: An LSWI-Based Method for Mapping Irrigated Areas in China Using Moderate-Resolution Satellite Data, Remote Sensing, 12, 4181, 10.3390/rs12244181, 2020.

Xie, Y. and Lark, T. J.: Mapping annual irrigation from Landsat imagery and environmental variables across the conterminous United States, Remote Sensing of Environment, 260, 112445, 10.1016/j.rse.2021.112445, 2021.

Xie, Y., Gibbs, H. K., and Lark, T. J.: Landsat-based Irrigation Dataset (LANID): 30-m resolution maps of irrigation distribution, frequency, and change for the U.S., 1997–2017, Earth Syst. Sci. Data, 2021, 1-32, 10.5194/essd-2021-207, 2021.

Xie, Y., Lark, T. J., Brown, J. F., and Gibbs, H. K.: Mapping irrigated cropland extent across the conterminous United States at 30 m resolution using a semi-automatic training approach on Google Earth Engine, ISPRS Journal of Photogrammetry and Remote Sensing, 155, 136-149, 10.1016/j.isprsjprs.2019.07.005, 2019.

Xiong, J., Thenkabail, P. S., Gumma, M. K., Teluguntla, P., Poehnelt, J., Congalton, R. G., Yadav, K., and Thau, D.: Automated cropland mapping of continental Africa using Google Earth Engine cloud computing, ISPRS Journal of

Photogrammetry and Remote Sensing, 126, 225-244, 10.1016/j.isprsjprs.2017.01.019, 2017.

Xu, X., Liu, J., Zhang, S., Li, R., Yan, C., and Wu, S.: Remote sensing-based monitoring dataset of land use and cover change over multiple periods in China (CNLUCC) (in Chinese). Resource and Environmental Science Data Center. DOI:10.12078/2018070201 [dataset], 10.12078/2018070201, 2018.

910   Yang, Y., Jin, Z., Mueller, N. D., Driscoll, A. W., Hernandez, R. R., Grodsky, S. M., Sloat, L. L., Chester, M. V., Zhu, Y.-G., and Lobell, D. B.: Sustainable irrigation and climate feedbacks, Nature Food, 4, 654-663, 10.1038/s43016-023-00821-x, 2023.

Yao, Z., Cui, Y., Geng, X., Chen, X., and Li, S.: Mapping Irrigated Area at Field Scale Based on the OPtical TRApezoid Model (OPTRAM) Using Landsat Images and Google Earth Engine, IEEE Transactions on Geoscience and Remote Sensing,
915   60, 1-11, 10.1109/TGRS.2022.3148274, 2022.

Yu, Z., Jin, X., Miao, L., and Yang, X.: A historical reconstruction of cropland in China from 1900 to 2016, Earth System Science Data, 13, 3203-3218, 10.5194/essd-13-3203-2021, 2021.

Zaveri, E. and B. Lobell, D.: The role of irrigation in changing wheat yields and heat sensitivity in India, Nature Communications, 10, 10.1038/s41467-019-12183-9, 2019.

920   Zeng, R. and Ren, W.: The spatiotemporal trajectory of US agricultural irrigation withdrawal during 1981-2015, Environmental Research Letters, 2022.

Zhang, C., Dong, J., and Ge, Q.: IrriMap_CN: Annual irrigation maps across China in 2000–2019 based on satellite observations, environmental variables, and machine learning, Remote Sensing of Environment, 280, 113184, 10.1016/j.rse.2022.113184, 2022a.

925   Zhang, C., Dong, J., and Ge, Q.: Mapping 20 years of irrigated croplands in China using MODIS and statistics and existing irrigation products, Scientific Data, 9, 10.1038/s41597-022-01522-z, 2022b.

Zhang, C., Dong, J., Xie, Y., Zhang, X., and Ge, Q.: Mapping irrigated croplands in China using a synergetic training sample generating method, machine learning classifier, and Google Earth Engine, International Journal of Applied Earth Observation and Geoinformation, 112, 102888, 10.1016/j.jag.2022.102888, 2022c.

930   Zhang, F., Zhang, T., Li, C., and Li, Z.: Cropland in China (in Chinese), China Agricultural University Press2021.

Zhang, L., Wang, W., Ma, Q., Hu, Y., and Zhao, Y.: CCropLand30: High-resolution hybrid cropland maps of China created through the synergy of state-of-the-art remote sensing products and the latest national land survey, Computers and Electronics in Agriculture, 218, 108672, 10.1016/j.compag.2024.108672, 2024.

Zhang, L., Xie, Y., Zhu, X., Ma, Q., and Brocca, L.: CIrrMap250: Annual maps of China's irrigated cropland from 2000 to
935   2020, 10.6084/m9.figshare.24814293.v1, 2023a.

Zhang, L., Zhang, K., Zhu, X., Chen, H., and Wang, W.: Integrating remote sensing, irrigation suitability and statistical data for irrigated cropland mapping over mainland China, Journal of Hydrology, 613, 128413, 10.1016/j.jhydrol.2022.128413, 2022d.

Zhang, L., Ma, Q., Zhao, Y., Chen, H., Hu, Y., and Ma, H.: China's strictest water policy: Reversing water use trends and

940 alleviating water stress, Journal of Environmental Management, 345, 118867, 10.1016/j.jenvman.2023.118867, 2023b.

Zhu, P. and Burney, J.: Untangling irrigation effects on maize water and heat stress alleviation using satellite data, Hydrology and Earth System Sciences, 26, 827-840, 10.5194/hess-26-827-2022, 2022.

Zhu, P., Burney, J., Chang, J., Jin, Z., Mueller, N. D., Xin, Q., Xu, J., Yu, L., Makowski, D., and Ciais, P.: Warming reduces
945 global agricultural production by decreasing cropping frequency and yields, Nature Climate Change, 10.1038/s41558-022-01492-5, 2022.

Zhu, X., Zhu, W., Zhang, J., and Pan, Y.: Mapping Irrigated Areas in China From Remote Sensing and Statistical Data, IEEE Journal of Selected Topics in Applied Earth Observations and Remote Sensing, 7, 4490-4504, 10.1109/JSTARS.2013.2296899, 2014.

950 Zuo, W., Mao, J., Lu, J., Zheng, Z., Han, Q., Xue, R., Tian, Y., Zhu, Y., Cao, W., and Zhang, X.: Mapping Irrigated Areas Based on Remotely Sensed Crop Phenology and Soil Moisture, Agronomy, 13, 1556, 10.3390/agronomy13061556, 2023.